nature communications

Article

https://doi.org/10.1038/s41467-026-72846-2

Simultaneous orthogonal cell engineering by a single CRISPR-Cas9 polyfunctional editor

Received: 28 April 2025

Accepted: 22 April 2026

Published online: 08 May 2026

Check for updates

Deborah Cipria[1,11], Tania Baccega[1,9,11], Miriana Rizzo[1], Piergiuseppe Quarato[1], Alice Reschigna[1,10], Rita El Khoury[2,3], Martino Alfredo Cappelluti[1], Sandra Ammann[4,5], Valeria Mollica Poeta[1], Matteo Conti[1], Sara Valsoni[1], Pietro Spinelli[6], Ivan Merelli[1,7], Toni Cathomen[4,5,8], Monica Casucci[2] & Angelo Lombardo[1,3]

The parallel disruption of multiple genes coupled with targeted transgene insertion offers a powerful strategy for more effective and precise cell engineering. However, such orthogonal editing involves the induction of multiple DNA breaks, raising safety concerns related to the risks of chromosomal translocations. Here, we present a polyfunctional CRISPR-Cas9-based strategy that enables both transgene insertion and epigenetic silencing at distinct genomic loci in a single treatment without inducing reciprocal chromosomal translocations. This is accomplished through an optimized all-in-one epigenome editor equipped with a catalytically active Cas9, whose endonuclease activity is selectively disabled at epigenetically silenced loci using truncated gRNAs. As a proof of concept, we demonstrate that this platform enables efficient multi-locus editing, including functional replacement of the endogenous TCR with a tumor-selective one, targeted insertion of a prototypic CAR with either a selectable marker or an immunomodulatory receptor into a TCR locus or a ubiquitously expressed gene, and durable, multiplexed epigenetic silencing of clinically relevant genes in primary human T cells. Polyfunctional editing establishes a versatile and safe framework for orthogonal editing, broadening the scope of genome and epigenome engineering in cancer immunotherapy and beyond.

The CRISPR-Cas9 system has emerged as a powerful platform for precise and versatile genome engineering[1]. The prototypic *Streptococcus pyogenes* Cas9 can deliver a DNA double-strand break (DSB) at a genomic site specified by a guide RNA (gRNA) containing a 20-nucleotide (nt) spacer sequence complementary to the intended target site[2,3]. The DSB activates the DNA Damage Response (DDR), which can be harnessed to insert a transgene into a predetermined genomic site through Homologous-Directed Recombination (HDR) with an exogenously provided donor DNA template. Alternatively, the DDR can be exploited to introduce frame-shift mutations in the coding sequence of a gene, a process often mediated by the error-prone Non-Homologous End Joining (NHEJ) pathway. The adoption of gRNA

[1]San Raffaele Telethon Institute for Gene Therapy, IRCCS San Raffaele Scientific Institute, Milan, Italy. [2]Innovative Immunotherapies Unit, Division of Immunology, Transplantation and Infectious Diseases, IRCCS San Raffaele Scientific Institute, Milan, Italy. [3]Vita-Salute San Raffaele University, Milan, Italy. [4]Institute for Transfusion Medicine and Gene Therapy, Medical Center—University of Freiburg, Freiburg, Germany. [5]Center for Cell and Gene Therapy Freiburg (CGF), Medical Center, University of Freiburg, Freiburg, Germany. [6]nChroma Bio Inc., Boston, MA, USA. [7]Institute for Biomedical Technologies, National Research Council, Segrate, Italy. [8]Faculty of Medicine, University of Freiburg, Freiburg, Germany. [9]Present address: Veneto Institute of Oncology IOV–IRCCS, Padua, Italy. [10]Present address: Department of Ophthalmology, LMU University Hospital, LMU Munich, Munich, Germany. [11]These authors contributed equally: Deborah Cipria, Tania Baccega. e-mail: lombardo.angelo@hsr.it

combinations has enabled parallel, orthogonal editing operations with high efficiency, such as multiplexed gene inactivation and locus-specific transgene insertion, facilitating the generation of cells with customized genetic programs. In the T-cell engineering space, this strategy has been extensively used to knock in a tumor-reactive T Cell Receptor (TCR) or a Chimeric Antigen Receptor (CAR) at an endogenous TCR locus while simultaneously inactivating genes involved in immune inhibitory pathways or allogeneic responses[4–7]. These T-cell products are under intense clinical investigation to treat various hematological and solid malignancies[8].

However, DSB induction raises safety concerns. Indeed, DSB repair can frequently lead to on-target genomic aberrations, ranging from large-scale rearrangements and deletions to the loss of entire chromosomes[9–11]. Furthermore, multiple breaks can be the source of reciprocal chromosomal translocations among the targeted loci[12–15]. In the context of T-cell engineering, these concerns are further exacerbated by the fact that translocations can persist long-term in transplanted patients[12], and that translocations involving the TCR genes - arguably the most common target in this field - are frequent drivers of certain hematological malignancies[16]. For these reasons, the field is transitioning toward editing technologies that operate independently from DSB induction, such as base editors[17]. These chimeric proteins perform a wide range of single-base conversions through the coordinated action of a nucleotide deaminase domain and a Cas9 variant with single-strand DNA (nick) cleavage activity. This platform has been used to install stop codons in different genes at high efficiencies, demonstrating promising results in early-phase clinical trials of gene-disrupted T cells[18,19]. However, the use of base editing can drastically reduce - but not fully abrogate - the risk of translocations. Indeed, recent studies have shown that nicks and/or intermediates of base deamination could be converted into DSBs, potentially leading to translocations at rates estimated to be as high as ~0.2%[15,20–22]. These frequencies may still have clinical relevance in transplantation settings involving high cell doses.

Epigenome editing with Engineered Transcriptional Repressors (ETRs) could provide a general solution to these problems, allowing multiplexed gene silencing without inducing DNA breaks[23]. ETRs consist of a catalytically deactivated Cas9 (dCas9) fused to epigenetic effector domains that possess histone-modifying (e.g., KRAB) and DNA methyltransferase (e.g., DNMT3A and its cofactor, DNMT3L) activities[23]. When targeted to the regulatory region of a gene, the ETRs deposit repressive epigenetic marks that induce local chromatin compaction, effectively silencing gene expression. Furthermore, as methylation at CpG dinucleotides can be inherited through cell mitosis, the ETR-targeted gene is maintained in a stably silenced state, as initially demonstrated in immortalized and primary cells[23,24], and recently confirmed also in mice and non-human primates[25–27]. Although well-suited for multiplexed gene silencing, the ETR platform lacks the orthogonal capabilities required for targeted transgene insertion, limiting its scope in cell engineering applications that require precise genetic addition. Here, we present a CRISPR-Cas9-based polyfunctional strategy that exploits gRNAs of different lengths and an all-in-one editor architecture to simultaneously program single-site multi-transgene insertion and multiplexed epigenetic silencing without inducing reciprocal chromosomal translocations. This approach proved to be highly effective in primary human T cells, offering a robust and safe platform for advanced orthogonal genome and epigenome editing.

Results

Development of the polyfunctional editing platform

Developing an orthogonal editor based on the CRISPR-Cas9 system poses the challenge of uncoupling its genetic and epigenetic editing activities at distinct loci. In this regard, previous studies have shown that Cas9 activity can be inactivated when coupled with a truncated gRNA[28] and that combinations of full-length and 5′-end truncated gRNAs can drive gene disruption and transcriptional activation at separate loci in cell lines[29,30] and transgenic mice[31]. To assess whether the ETR technology can impose efficient and durable epigenetic silencing (epi-silencing) with truncated gRNAs, we developed a panel of gRNAs differing only in spacer length (from 20 to 10-nt) and targeting exon 1 of the human *Beta-2 Microglobulin* (*B2M*) gene (Fig. 1A). We then separately transfected these gRNAs along with a previously described triple ETR combination[23,25] in a K-562 cell line encoding tdTomato from the *B2M* locus[23]. On day 30 post-treatment, we analyzed the cells by flow cytometry for $B2M^{tdTomato}$ expression. These experiments showed that ETRs retained epi-silencing activity with almost all tested gRNAs. Indeed, except for the 10-nt-long gRNA, all other truncated guides were similarly effective as the full-length (20-nt) gRNA (Figs. 1B and S1A). We then assessed the dependence of canonical gene editing on gRNA length. We thus performed the above experiment with a catalytically competent Cas9 and found loss of editing activity already at gRNA lengths ≤16-nt (Fig. 1B). Truncation of another *B2M* gRNA confirmed retention of epi-silencing at gRNA lengths that abrogate Cas9 endonuclease activity (Figs. S1B, C). These data reveal a more pronounced gRNA length dependency for Cas9 than for ETRs, offering a window of opportunity for developing polyfunctional editors (a design hereafter collectively referred to as poly-editors).

Thus, we restored the endonuclease activity into the dCas9 domain of the ETRs and assessed whether these poly-editors could simultaneously program epi-silencing of *B2M* and targeted insertion of an eGFP-expression cassette into the safe harbor locus *AAVS1*[32] (Fig. 1C). In these settings, we used 16-nt- and 20-nt-long gRNAs for *B2M* and *AAVS1*, respectively. A single treatment with the poly-editor resulted in around 41% of cells that were only $B2M^{tdTomato}$-negative and 8% of cells that were both $B2M^{tdTomato}$-negative and eGFP-positive (Figs. 1D and S1D), indicating double editing in the latter cell population. The remaining cells were either expressing $B2M^{tdTomato}$ (~49%) or double-positive for $B2M^{tdTomato}$ and eGFP (~2%). Molecular analyses of sorted double-edited cells revealed de novo DNA methylation (Figs. 2A and S2A) and no genetic scars at *B2M* (Fig. 2B), confirming genuine epigenetic silencing of this gene. On the other hand, the *AAVS1* locus exhibited a high mutational burden (i.e., small insertions and deletions, indels; Fig. 2B) a finding in line with the NHEJ-mediated repair of the *AAVS1* alleles lacking insertion of the eGFP cassette. In these experimental settings, the polyfunctional editor retained similar gene targeting activity as the parental Cas9 protein (Fig. S2B). To assess whether the poly-editor could also depose DNA methylation at the *AAVS1* locus or within the targeted cassette, we initially profiled the methylation status of the locus before and after cassette insertion and found no major differences (Fig. 2C). The eGFP cassette, including its promoter, displayed a low methylation profile (Fig. 2D), consistent with active transgene expression. These findings were comparable to those obtained following conventional Cas9-mediated cassette insertion, indicating that the poly-editor did not alter the methylation status of the targeted locus and the cassette. In line with these results, eGFP was expressed at similar levels in poly- and gene-edited cells (Fig. S2C). Finally, we detected and quantified the occurrence of reciprocal translocations between *B2M* and *AAVS1* using ad hoc-designed junction PCR approaches. In contrast to cells treated with Cas9 and 20nt-long gRNAs for both genes, in which the reciprocal translocation events ranged from 0.4% to 1.5%, poly-edited cells showed no translocations above background levels (Figs. 2E and S2D). Overall, these data show that gRNAs of different lengths can be used to promote durable gene silencing and targeted transgene insertion when coupled with Cas9-equipped epigenetic editors.

https://doi.org/10.1038/s41467-026-72846-2

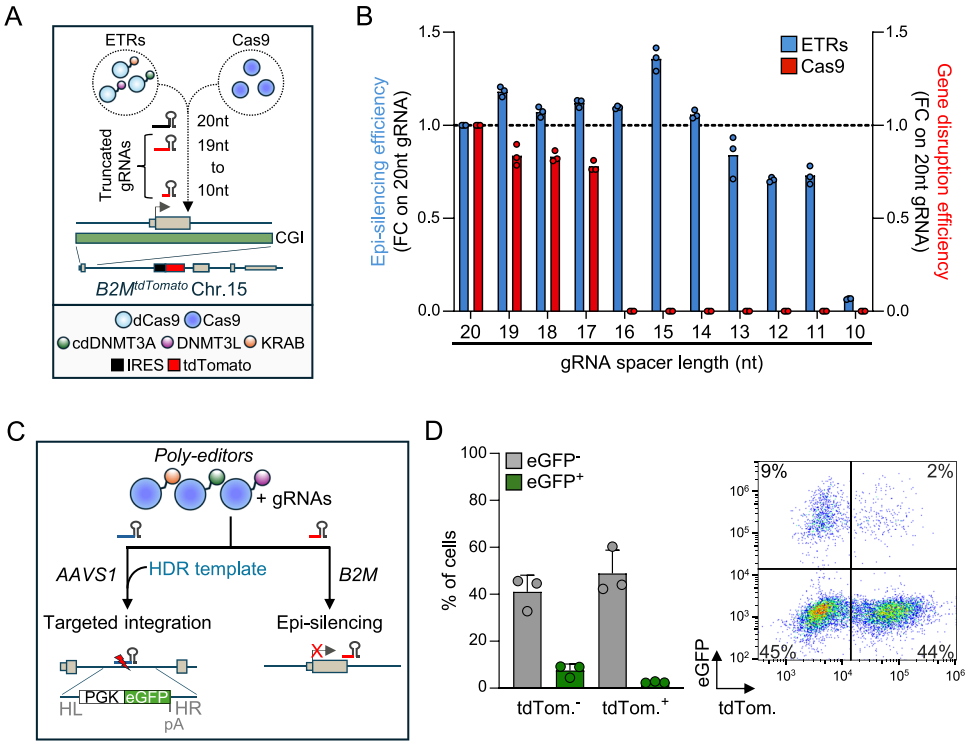

Fig. 1 | Development of the polyfunctional editing strategy in *B2M*^{tdTomato} K-562 cells. A Diagram of the experimental procedure used to assess the efficiencies of epi-silencing or disruption of the *B2M*^{tdTomato} gene using gRNAs with progressively shorter spacer sequences (ranging from 20 to 10nt) and either the triple ETR combination (ETRs) or Cas9, respectively. The genetic makeup of the *B2M* locus is depicted at the bottom. The triple ETR combination consists of dCas9 fused to either the KRAB domain of the human ZNF10, the catalytic domain of human DNMT3A (cdDNMT3A), or human DNMT3L. CGI: CpG Island. IRES: Internal Ribosome Entry Site. **B** Bar graph showing the efficiencies of epi-silencing (left-hand *y*-axis, blue bars) or disruption (right-hand *y*-axis, red bars) of *B2M*^{tdTomato} with the indicated gRNAs. Data are shown as Fold Change (FC) relative to samples treated with the full-length (20nt) *B2M* gRNA$^{B\#6}$ (mean ± SD of 3 experimental replicates). Epi-silencing efficiencies were calculated by measuring the percentage of *B2M*^{tdTomato}-negative cells by flow cytometry, while gene disruption efficiencies were calculated by measuring the percentage of small insertions and deletions (indels) at the locus by T7 assay. **C** Schematic representation of the polyfunctional editing procedure used to epi-silence *B2M*^{tdTomato} and insert an eGFP-expression cassette into *AAVS1* by HDR. Note that the poly-editors contain a catalytically active Cas9. The editing components were delivered into the K-562 *B2M*^{tdTomato} cells by plasmid-based transfection. HL and HR: homology left and homology right for HDR. PGK: promoter of the human Phosphoglycerate Kinase gene. eGFP: enhanced Green Fluorescent Protein. **D** Left: percentages of eGFP-negative (gray bars) and eGFP-positive (green bars) cells within tdTomato-negative or -positive cells (mean ± SD of 3 independent experiments). Cells were analyzed by flow cytometry 20 days after nucleofection with plasmids encoding the poly-editors and the 20nt and 16nt gRNAs targeting *AAVS1* and *B2M*, respectively. Right: representative flow cytometry dot plot of K-562 *B2M*^{tdTomato} cells treated with the poly-editors and the combination of gRNAs. Graphs were generated using GraphPad Prism (GraphPad Software). Source data are provided as a Source Data file.

Platform optimization for more efficient polyfunctional editing in T cells

We then translated these findings into primary human T lymphocytes. In search for a more efficient gRNA to silence *B2M*, we initially tested nine full-length guides distributed across the CpG Island (CGI) of this gene (Fig. 3A). To our surprise, none of these gRNAs - including the one used in the K-562 reporter cell line - were able to induce durable *B2M* epi-silencing in T cells (Fig. 3A). This result prompted us to consider co-targeting the *B2M* promoter with multiple gRNAs. We thus conducted a gRNA screen in T cells, testing all possible pairwise combinations of gRNAs ($n = 36$). Unlike the previous experiment with individual gRNAs, most of the pairs induced detectable *B2M* epi-silencing (Fig. 3B). The best-performing pair consisted of the guide used in the reporter cell line (namely, gRNA$^{B\#6}$) and an upstream-binding gRNA (namely, gRNA$^{B\#2}$), resulting in ~40% of durable *B2M* epi-silencing (Figs. 3C and S3A). To further increase these efficiencies, we decided to develop improved ETR designs. To this end, we followed a stepwise optimization approach, in which we first tested different protein linkers[33] and then explored alternative effector domains[24,34] in various positions relative to dCas9 (Fig. 3D). Given the positive results obtained with all-in-one fusion ETRs[24–27,35,36], we applied a similar optimization strategy to these architectures as well. Testing these variants ($n = 27$ different constructs for the triple ETR combination and 8 for the all-in-one tripartite ETRs) in the *B2M*^{tdTomato} K-562 cell line with the 20-nt gRNA$^{B\#6}$ indicated a tripartite design that exhibited a 2.1-fold higher epi-silencing efficiency compared to the original triple ETR combination (Fig. 3D). The improved tripartite ETR contains an obligate heterodimer between the catalytic domain of human DNMT3A and a shorter version of the murine Dnmt3l[24], along with the KRAB domain from the ZIM3 repressor[34], both connected to dCas9 by XTEN linkers. In the above settings, this architecture proved to be highly specific, with no genes other than *B2M* being significantly down-regulated by the treatment (Figs. 3E and S3B). Notably, this high specificity profile was also maintained with the 16-nt gRNA$^{B\#6}$, indicating that guide truncation does not increase the off-targeting activity of the editor. Comparing the epi-silencing efficiency of the selected tripartite ETR with the parental ETR combination in different cell lines and primary T cells, and across different loci, confirmed the superiority of the improved architecture, reaching ~80% of long-term stable silencing of *B2M* and two other genes in T cells (Figs. 4A and S4A–D). In line with the mechanism of action of the ETR technology, both treatments resulted in a significant increase in the levels of methylation across the *B2M* CGI, including the gene promoter (Fig. 4B). Whole transcriptomic analysis of T cells in which *B2M* was epi-silenced using full-length or truncated gRNAs showed a > 1.8-fold reduction in *B2M* levels (Fig. S4E) and no differentially expressed genes between the two experimental

https://doi.org/10.1038/s41467-026-72846-2

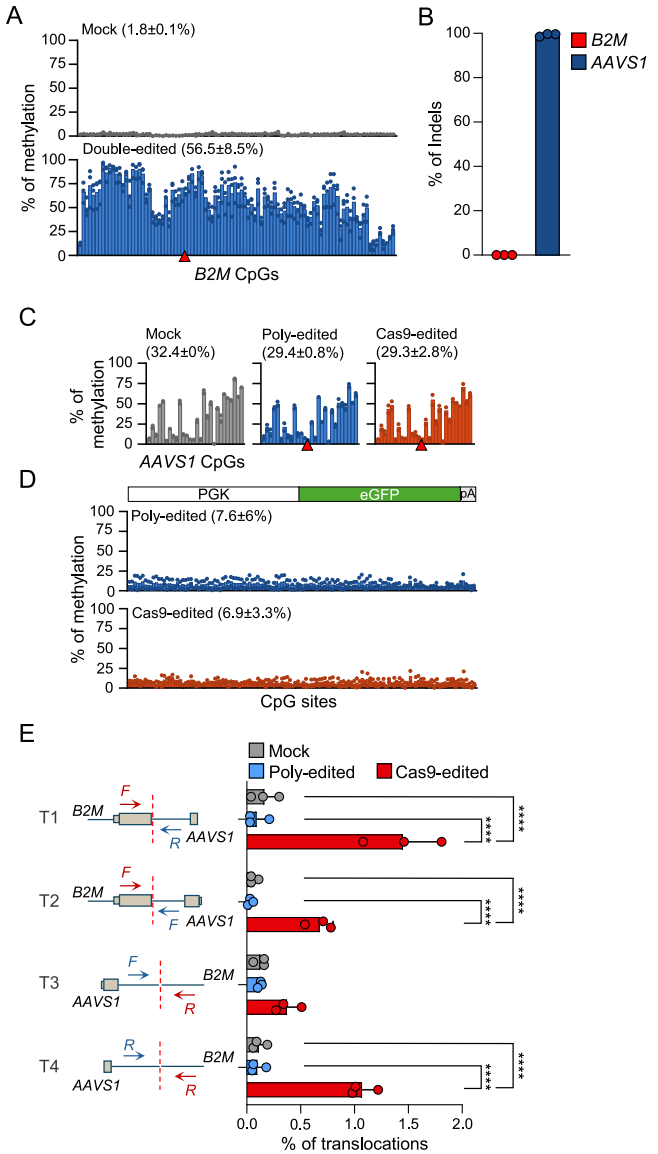

Fig. 2 | Molecular characterization of polyfunctional edited *B2M*^{tdTomato} K-562 cells. A CpG methylation profile across the *B2M* promoter (Chr.15: 44,710,818-44,712,607) of mock-treated and double-edited cells (mean ± SD of 3 experimental replicates), with mean methylation levels across the investigated region indicated in brackets. Red triangle indicates the 16nt-long *B2M* gRNA target site. **B** Percentage of indels at *B2M* (red bar) and *AVVS1* (blue bar) in sorted poly-edited cells (mean ± SD of 3 experimental replicates), as measured by deep-sequencing. **C** CpG methylation profiles across the *AAVS1* locus (Chr. 19: 55,115,172-55,116,228) in mock-treated, poly-edited, and Cas9-edited cells (mean ± SD of 2 independent experiments), with mean methylation levels across the investigated region indicated in brackets. Red triangles indicate the *AAVS1* gRNA target site. **D** CpG methylation profiles of the eGFP cassette in poly- and Cas9-edited cells (mean ± SD of 2 independent experiments), with mean methylation levels across the investigated region indicated in brackets. **E** Bar plot showing the percentages of translocations between *B2M* and *AAVS1* (from T1 to T4, as depicted in the left schematics) in Cas9- (red bars), poly-edited (blue bars), and mock-treated (gray bars) cells (mean ± SD of 3 independent experiments). F and R: forward and reverse primers, in color code for *B2M* (red) and *AAVS1* (blue). ****$p < 0.0001$ by 2-way ANOVA with Tukey's multiple comparisons test. Graphs were generated using GraphPad Prism (GraphPad Software). Source data are provided as a Source Data file.

conditions (Fig. 4C), further confirming the high specificity of these gRNAs, also in their truncated configuration.

Thus, we constructed a polyfunctional editor based on the improved tripartite ETR architecture and empirically determined the optimal truncation length for gRNA$^{B\#2}$ in the K-562 reporter cell line and T cells (Fig. S5A, B). Having established these reagents, we co-transfected activated primary T cells with the mRNA encoding the polyfunctional editor, the two truncated *B2M* gRNAs, and the full-length gRNA for *AAVS1*. Immediately thereafter, we transduced these cells with an Adeno-Associated Viral (AAV) vector containing the donor DNA template for targeted integration of an eGFP expression cassette into *AAVS1*[37] (Fig. 5A). Longitudinal flow cytometry analysis showed that approximately 30% of treated cells were both B2M-negative and eGFP-positive (Fig. 5B and S5C). These efficiencies were stable for up to 31 days post-treatment, when the experiment was terminated. At this time point, ~30% or 15% of the remaining cells were either single B2M-negative or single eGFP-positive, respectively. Endpoint molecular analyses demonstrated high levels of DNA methylation (Fig. 5C) and absence of indels at the *B2M* locus (Fig. 5D), directly correlating *B2M* silencing with epi-editing. Comparing the DNA methylation profile of the *AAVS1* locus before and after cassette insertion revealed a marked reduction in the methylation levels following both poly-editing and conventional Cas9-mediated gene targeting *vs.* mock-treated controls (Figs. 5E and S5D). The eGFP cassette was largely devoid of CpG methylation in both conditions (Fig. 5F), a finding consistent with similar eGFP expression profiles between poly- and Cas9-edited cells (Fig. S5E). The rate of chromosomal translocations between *AAVS1* and *B2M* remained at background levels in poly-edited cells, whereas it cumulatively reached around 1.8% in Cas9-treated samples (Fig. 5G). Altogether, these results validated the polyfunctional editing strategy in primary T cells, providing proof-of-principle of its safety and efficacy.

Polyfunctional editing allows multiplexed T-cell engineering

We assessed the portability of polyfunctional editing to other loci of potential relevance for cancer immunotherapy. Here, we exploited a gene-targeting strategy designed to reconstitute a NY-ESO-1-specific TCR after its insertion into exon 1 of the *T Cell Receptor Alpha Constant* (*TRAC*) gene[5]. In allogeneic settings, this strategy has the additional advantage of knocking out the endogenous TCR through the gene-targeting procedure[38], thereby preventing graft-versus-host disease[39]. However, engineered cells remain vulnerable to elimination by the host immune system, which recognizes mismatches in the highly polymorphic Human Leukocyte Antigens (HLA) class I molecules of grafted cells. To mitigate this issue, researchers are considering genetic inactivation of *B2M*[40], whose protein product is a determinant of cell-surface expression of HLA class I molecules. Thus, we built a module that combines targeted insertion of the NY-ESO-1 TCR into *TRAC* and epi-silencing of *B2M* using full-length and truncated gRNAs (Fig. 6A), respectively. The donor DNA template for targeted insertion of the NY-ESO-1 TCR into *TRAC* was delivered into T cells via AAV vectors. This procedure resulted in three cell populations, with NY-ESO-1 TCR−positive cells accounting for ~28% (Figs. 6B and S6A). The two remaining populations were either negative or positive for cell-surface expression of the endogenous TCRs (39% *vs.* 32%, respectively). The appearance of TCR-negative T cells likely reflected NHEJ-mediated disruption of the single functioning *TRAC* allele. Within the NY-ESO-1 TCR−positive cells, around 65% of them lost B2M expression. To further improve the gene targeting efficiencies, we used an HDR enhancer, obtaining a 2.8-fold increase in the percentage of NY-ESO-1 TCR-positive cells (Figs. 6C, D and S6B), with a concomitant reduction in the percentage of TCR-negative cells, a finding in line with a skewing of the DDR towards HDR. Notably, this treatment had no negative impact on the overall efficiency of *B2M* epi-silencing, which reached ~82% within the NY-ESO-1 TCR-positive cells. CpG methylation profiling of *TRAC* sequences flanking the cassette insertion site revealed a comparable reduction in methylation in both poly- and Cas9-edited cells relative to mock-treated cells (Fig. 6E), with minimal methylation across the transgenic NY-ESO-1 TCR (Fig. 6F). In line with this, equal

https://doi.org/10.1038/s41467-026-72846-2

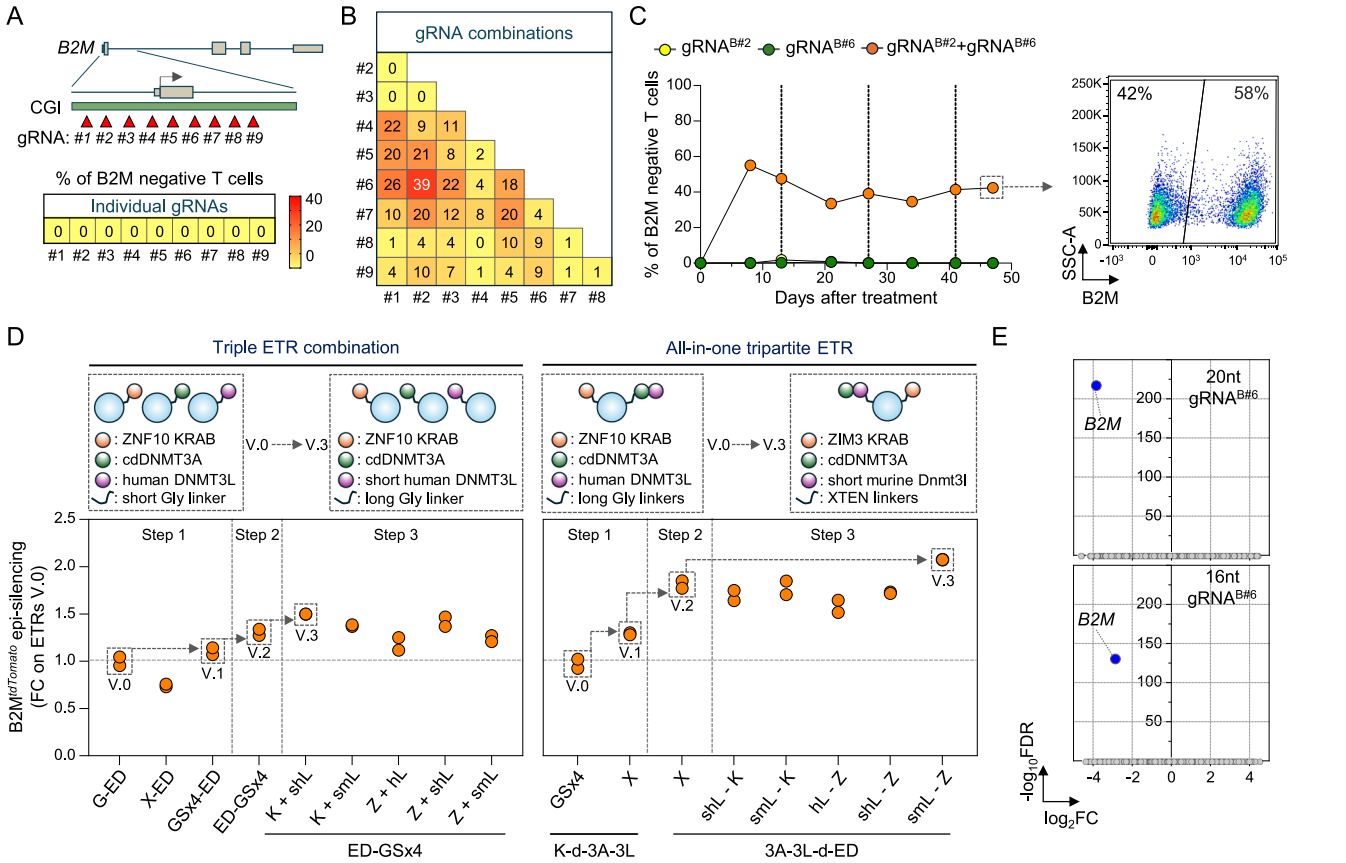

Fig. 3 | Development of an improved ETR design. A Top: to-scale schematic of the *B2M* gene with an enlarged view of the promoter region showing the target sites of the nine gRNAs tested (red triangles). Bottom: heat map showing the percentage of B2M-negative T cells by flow cytometry on day 27 post-transfection with the indicated gRNAs and mRNAs encoding the triple ETR combination. Data were normalized to the percentage of B2M-negative cells in mock-treated T cells. **B** Heat map showing the percentage of B2M-negative T cells after treatment with the indicated gRNA combinations, analyzed as in (**A**). **C** Left: percentage of B2M-negative T cells from the indicated conditions in (**B**) over 47 days post-treatment. Vertical dashed lines indicate T-cell restimulation. Colored dots indicate either individual gRNAs or their combination. Right: representative flow cytometry dot plot of T cells treated with the triple ETR combination and gRNA$^{B\#2}$ + gRNA$^{B\#6}$. SSC-A: Side Scatter Area. **D** Top: schematic representation of the triple ETR combinations (left) and all-in-one ETRs (right) before (V.0) and after (V.3) optimization. Bottom: fold-change in the efficiency of *B2M*^{dTomato} epi-silencing between the new ETR architectures and either the initial triple ETR combination or the tripartite ETR (V.0). Epi-silencing efficiencies were measured by flow cytometry 21 days after plasmid transfection (mean ± SD, $n = 2$ experimental replicates). Construct optimization was carried out as follows: selection of the best-performing interdomain linker (Step 1), inversion of the position of the Effector Domain(s) (ED) relative to dCas9 (Step 2) and testing of alternative EDs (Step 3). EDs tested: ZNF10-KRAB (K), ZIM3-KRAB (Z), human full-length DNMT3L (hL), short versions of the human DNMT3L (shL) or murine Dnmt3l (smL), and the catalytic domain of the human DNMT3A (3A). Linkers tested: GSGGG (G, short Gly linker), $(GGGGS)_4$ (GSx4, long Gly linker), and XTEN-based linkers (X), with XTEN16 connecting KRAB to dCas9 and XTEN80 linking the DNA methylation domains to dCas9. **E** Volcano plots showing differential gene expression between mock-treated and *B2M* epi-silenced cells with the 20nt- or the 16nt-long *gRNA*$^{B\#6}$ gRNAs ($n = 3$ experimental replicates). Genes significantly down-regulated (FDR ≤ 0.05) are indicated in blue, while genes not differentially expressed are in gray. Graphs were generated using GraphPad Prism (GraphPad Software). Source data are provided as a Source Data file.

expression of the NY-ESO-1 TCR was measured in both editing conditions (Fig. S6C, D). To assess the functionality and antigen selectivity of the poly-edited T cells, we co-cultured them with a Gaussia luciferase-expressing NALM-6 cell line[41] (hereafter referred to as GLuc.NALM-6) that was further engineered to express NY-ESO-1 (GLuc.NALM-6 NY$^+$; Fig. S6E). This cell line also encodes the appropriate HLA to present the NY-ESO-1 peptide to the cognate TCR. In these settings, poly-edited T cells efficiently killed the GLuc.NALM-6 NY$^+$ cells across a wide range of effector-to-target ratios while sparing their negative counterparts (Fig. 6G, left panel). Killing was associated with the release of pro-inflammatory cytokines (Fig. 6G, right panels). Comparable results were obtained using control T cells engineered solely to express the NY-ESO-1 TCR from the *TRAC* locus (TCR^{NY} T cells; Fig. 6G, left and right panels).

We then assessed whether polyfunctional editing could support multiplexed epi-silencing. To this end, we selected the *Tet methylcytosine dioxygenase 2* (*TET2*) gene since its knockout has been proposed to counteract T cell exhaustion in vivo[42,43]. In preparation for poly-functional editing, we selected full-length gRNAs against *TET2* (Fig. 7A). Informed by our previous results showing a beneficial effect of gRNA combination, we decided here to adopt a funnel selection approach. Specifically, we identified effective quadruple gRNA combinations and then, to reduce the number of gRNAs required for polyfunctional editing, deconvoluted these combinations into pairs and individual gRNAs. The initial screening experiments showed that *TET2* responded well to epi-silencing, with several gRNA combinations reducing >80% the levels of the *TET2* transcripts. Further deconvolution of two effective quadruple combinations (namely, J + E and J + G) identified an equally performing pair (namely, J; Fig. 7B). Conversely, none of the individual gRNAs tested were as efficient as their parental quadruple combinations. Epi-silencing of *TET2* with the J gRNA pair was associated with increased DNA methylation (Fig. 7C). Based on these findings, we combined targeted insertion of the NY-ESO-1 TCR into *TRAC* with epi-silencing of *B2M* and *TET2* in a single polyfunctional procedure (Fig. 7D). Given that our findings showed a loss of Cas9 activity for gRNAs shorter than 17-nt, we used 14-nt-long gRNAs for the

https://doi.org/10.1038/s41467-026-72846-2

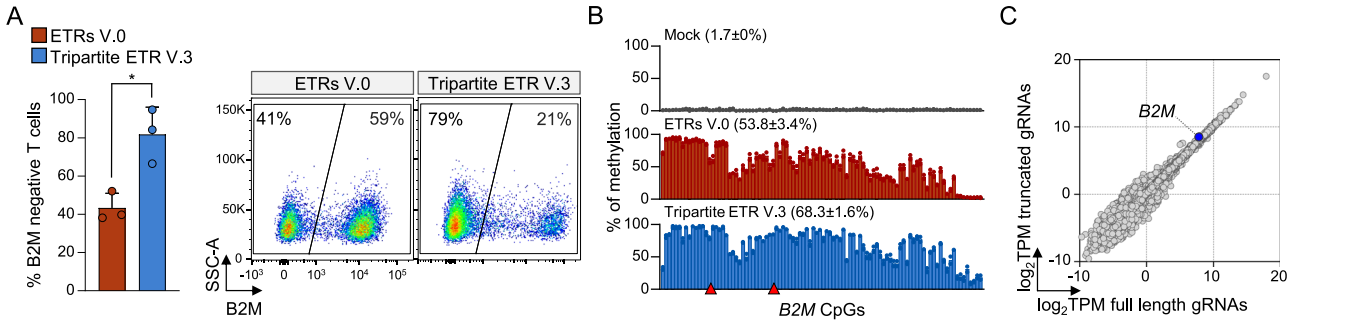

Fig. 4 | Efficient epi-silencing in primary human T lymphocytes with the improved ETR design. A Left: percentage of B2M-negative T cells measured by flow cytometry at day 29 post-treatment with the selected pair of *B2M* gRNAs and either the original triple ETR combination (V.0; red bar) or the optimized tripartite ETR (V.3; blue bar) (mean ± SD of 3 blood donors). *$p = 0.02503$ by unpaired two-tailed Welch's t-test. Right: representative flow cytometry dot plots of T cells treated as indicated. **B** CpG methylation profiles across the *B2M* promoter region in T cells from (**A**) (mean ± SD of 2 independent blood donors), with mean methylation levels across the investigated region indicated in brackets. Red triangles indicate the *B2M* gRNAs target sites. **C** Scatter plot comparing whole-transcriptome analyses of T cells treated with the tripartite ETR and either full-length or truncated *B2M* gRNAs ($n = 2$ experimental replicates). Data are expressed as $\log_2$ of Transcripts Per Million (TPM) of mapped reads. Graphs were generated using GraphPad Prism (GraphPad Software). Source data are provided as a Source Data file.

epi-silencing of *TET2*. Consistent with the results obtained for *B2M*, full-length and truncated *TET2* gRNAs displayed a comparable specificity profile (Figs. 7E and S7A). After poly-editing, >70% of treated T cells expressed the NY-ESO-1 TCR, nearly two-thirds of which were also *B2M*-negative (Fig. 7F and S7B). In treated cells, the *TET2* and *B2M* transcripts were reduced by approximately 10- and 4-fold (Fig. 7G), respectively. These triple-edited cells retained similar killing activity and antigen specificity as TCR^{NY} T cells when cultured with GLuc.-NALM-6 cells expressing or not NY-ESO-1 and released pro-inflammatory cytokines in response to antigen recognition (Fig. 7H). Overall, these data support the use of polyfunctional editing for efficient TCR replacement and multiplexed epi-silencing in T cells.

Polyfunctional editing is compatible with CAR-T cell engineering

We assessed the potential of polyfunctional editing as a strategy for CAR-T cell engineering. At first, we devised a procedure that foresees targeting of a composite cassette co-expressing the CD19–28ζ CAR and the truncated human Low-affinity Nerve Growth Factor Receptor (ΔLNGFR) selection marker into the *TRAC* locus, with co-epi-silencing of *B2M* and *TET2* (Fig. 8A). In these settings, ~81% of bulk-treated T cells simultaneously gained expression of ΔLNGFR and lost endogenous TCR expression (Figs. 8B and S8A). Within this population, ~64% of cells resulted negative for B2M expression. Transcriptional analyses further showed a marked reduction in *TET2* (6-fold) and *B2M* (4-fold) mRNA levels (Fig. 8C), indicating highly efficient triple-editing in these cells. When co-cultured with GLuc.NALM-6, poly-edited T cells demonstrated equivalent activity to T cells engineered solely to express the same CD19–28ζ CAR:ΔLNGFR from the *TRAC* locus (CAR-$T^{\Delta LNGFR}$ cells), both in terms of cytotoxic activity and pro-inflammatory cytokine production (Fig. S8B). Notably, similar results were obtained upon injecting the two engineered T cell populations into NSG mice bearing GLuc.NALM-6 (Fig. 8D). In contrast with mock-treated T cells, both engineered CAR-T cell populations equally and effectively controlled tumor growth and extended mice survival (Figs. 8E and S8C). These responses were accompanied by a progressive expansion in the number of circulating human T cells over time (Fig. S8D), which displayed an activated effector phenotype consistent with sustained antitumor activity (Fig. S8E, F), while preserving a substantial fraction of stem and central memory subsets. Moreover, these cells produced pro-inflammatory cytokines before leukemia regression (Fig. S8G). Next, we used CAST-Seq[10] to detect chromosomal aberrations at the *TRAC* locus, including translocations occurring between this gene and either *B2M* and *TET2*, or with the Off-Target (OT) sites of all gRNAs (Fig. 8F and Supplementary Data 1). These data were compared with those from conventional Cas9-mediated gene disruption (triple-KO). As expected, triple-KO cells harbored several translocations, including those among the three intended target genes, and between *TRAC* and either the OT sites of its gRNA ($n = 10$ loci) or those from the *TET2* gRNA ($n = 7$ loci). No translocations involving OT sites of the *B2M* gRNA were found in these analyses. By contrast, poly-edited T cells showed no translocations between *TRAC* and the two other intended target genes, and only a single translocation between *TRAC* and an OT site of its gRNA. Given the gene editing activity of the two editors, comparable efficiencies and profiles of genomic aberrations (large deletions and inversions) at the *TRAC* locus were found in both experimental conditions (Figs. 8G and S8H). The overall number of translocation events in poly-edited cells was >3-log lower than in triple-KO cells (Fig. 8G). These data further confirmed that truncated gRNAs disable Cas9-nuclease activity at the epi-silenced genes.

We also assessed the versatility of the polyfunctional platform by designing another allogenic module encompassing: (i) genetic inactivation of *B2M* through the insertion of a cassette encoding the CD19–28ζ CAR and a single-chain HLA-E trimer (scHLA-E)[44]. This single-step engineering enables constitutive and robust expression of the targeting receptor (i.e., the CAR) from the *B2M* promoter while partially shielding the otherwise HLA class I-negative cells from NK-mediated lysis through the expression of the invariant scHLA-E molecule[45,46]; (ii) epi-silencing of the *CD3 Delta* (*CD3D*) subunit of the TCR complex, resulting in the absence of this complex from the cell surface, and of the *Transforming Growth Factor Beta Receptor 2* (*TGFBR2*) gene, whose inhibition or genetic inactivation is emerging as a potential strategy to desensitize immune cells to TGF-β derived from the hostile tumor microenvironment[47–50]. We exploited the above-described screening paradigms to select effective full-length gRNAs pairs for epi-silencing of *CD3D* and *TGFBR2* (Fig. S9A, B) and then confirmed that truncation did not alter their specificity profile (Figs. 9A and S9C). For *CD3D* epi-silencing, we also detected a significant reduction in the expression of its paralog, *CD3G*, with which it shares regulatory sequences. Based on their efficacy and specificity, we used these truncated guides together with a full-length *B2M* gRNA targeting exon 1 of the gene (namely $gRNA^{B\#5}$) to perform poly-functional editing in primary human T cells (Fig. 9B), delivering the donor DNA template by AAV. This procedure yielded ~80% of cells double negative for endogenous HLA expression and CD3 (Figs. 9C and S9D), with nearly all of them co-expressing CD19–28ζ CAR and scHLA-E. Molecular analyses showed a strong reduction in the levels of *CD3D* and *TGFBR2* transcripts (Fig. 9D). Accordingly, the regulatory region of these two

https://doi.org/10.1038/s41467-026-72846-2

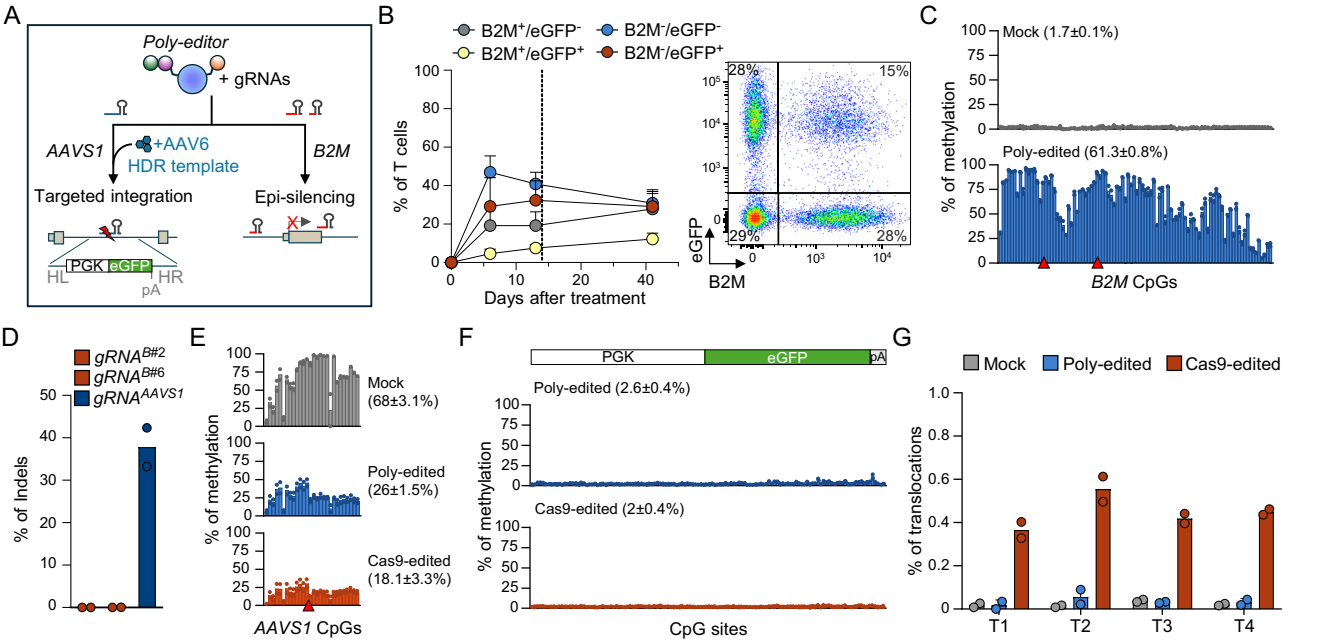

Fig. 5 | Tripartite ETR mediates polyfunctional editing in primary human T cells. A Schematic of the polyfunctional editing procedure used to epi-silence *B2M* and insert an eGFP-expression cassette into *AAVS1*. The editing machinery was delivered into T cells by RNA nucleofection, while the donor DNA template for HDR by the Adeno-Associated Viral vector Serotype 6 (AAV6). **B** Left: percentages of the indicated T cell populations as measured by flow cytometry over 31 days post-polyfunctional editing (mean ± SD of 6 blood donors). $B2M^+/eGFP^-$: B2M-positive, eGFP-negative cells (gray dot); $B2M^+/eGFP^+$: B2M-positiive, eGFP-positive cells (yellow dot); $B2M^-/eGFP^-$: B2M-negative, eGFP-negative cells (blue dot); $B2M^-/eGFP^+$: B2M-negative, eGFP-positive cells (red dot). Right: representative flow cytometry dot plot of poly-edited T cells. **C** CpG methylation profiles across the *B2M* promoter region of mock-treated and poly-edited T cells from (**B**) (mean ± SD of 2 blood donors), with mean methylation levels across the investigated region indicated in brackets. Red triangles indicate *B2M* gRNA target sites. **D** Percentage of indels at the two *B2M* gRNA target sites (red bars) and at the *AAVS1* gRNA target site (blue bar) in poly-edited cells from (**B**) (mean ± SD of 2 blood donors). **E**, **F** CpG methylation profiles of the *AAVS1* locus (panel **E**) and the eGFP cassette (panel **F**) in T cells treated as indicated (mean ± SD of 2 blood donors), with mean methylation levels across the investigated regions indicated in brackets. **G** Percentage of translocations between *B2M* and *AAVS1* in Cas9- (red bars), poly-edited (blue bars), and mock-treated (gray bars) T cells 6 days after treatment (mean ± SD of 2 blood donors). Graphs were generated using GraphPad Prism (GraphPad Software). Source data are provided as a Source Data file.

genes gained CpG methylation (Fig. 10A, B). At variance with *B2M*, no signs of genetic editing were observed at the two epi-silenced genes (Fig. 10C). Poly-editor-mediated cassette insertion at *B2M* resulted in the acquisition of CpG methylation predominantly downstream of the cassette (Fig. 10D), a finding also observed following standard Cas9-mediated gene targeting. Despite the higher methylation levels in poly-edited cells, expression of the scHLA-E:CD19–28ζ-CAR was comparable in the two editing conditions (Fig. S10A, B). CAST-Seq analysis revealed no reciprocal chromosomal translocations among the three intended target genes in poly-edited cells, while these events were present in triple-KO cells (Fig. 10E and Supplementary Data 1). In the latter conditions, three other translocations were found between *B2M* and one OT site of each gRNAs. Among these translocations, the one involving *B2M* and the single OT of its gRNA was also present in poly-edited cells. Similar levels of *B2M* genomic aberrations were found in gene- and poly-edited cells (Fig. S10C), with a > 3-log lower number of translocation events in poly-edited cells *vs.* triple-KO cells (Fig. 10F). Finally, we performed in vitro functional assays confirming that these poly-edited cells were also able to efficiently kill and produce pro-inflammatory cytokines upon encountering GLuc.NALM-6 cells, at levels comparable to those of control CAR-$T^{scHLA\text{-}E}$ cells (Fig. 10G). Poly-edited cells retained epi-silencing of both *CD3D* and *TGFBR2* after tumor killing (Fig. 10H). Altogether, these data confirmed the portability of the polyfunctional editing platform for efficient and safe CAR-T cell engineering.

Discussion

Here, we present a strategy to introduce orthogonal genome and epigenome edits at multiple genomic sites without inducing reciprocal chromosomal translocations. This strategy revolves around the use of a single-molecule, CRISPR-Cas9-based editor, equipped with both DNA cleavage and epigenetic activities. To effectively uncouple these functions at distinct genomic sites, we employed an endonuclease switch approach that exploits gRNAs of different lengths to deactivate Cas9 at the genes designated for epigenetic silencing while allowing transgene insertion in another locus. This approach confers a high degree of gene discrimination and specificity to the platform, enabling the generation of multi-edited T cells. To prevent epi-silencing of the transgene-bearing gene, we initially selected target sites that are either within regions that lack a regulatory role in gene transcription, outside the predicted window of activity of the editor[24], and/or exhibit low CpG dinucleotide density, such as *AAVS1* and *TRAC*. The latter feature prevents the establishment of a stable epigenetic memory based on DNA methylation while restraining its spreading from the poly-editor target site into the promoter of the transgene-bearing gene. In this setting, the exogenous cassette is also shielded from both cleavage and silencing, as it lacks the editor binding site. We further showed that genomic regions responsive to epi-silencing, such as the *B2M* CGI, could also be considered as cassettes integration sites. Here, the use of a single gRNA rather than combinations, together with the conceivably rapid genetic disruption of the editor-binding site through cassette insertion, may protect these genes from unintended epi-silencing. Despite these considerations, in T cells, we observed measurable changes in the CpG methylation status of the cassette-bearing loci after polyfunctional editing. However, their magnitudes and profiles were comparable to those observed following conventional Cas9-mediated cassette insertion. Therefore, these effects may reflect a reconfiguration of the loci driven by the exogenous cassettes and/or

https://doi.org/10.1038/s41467-026-72846-2

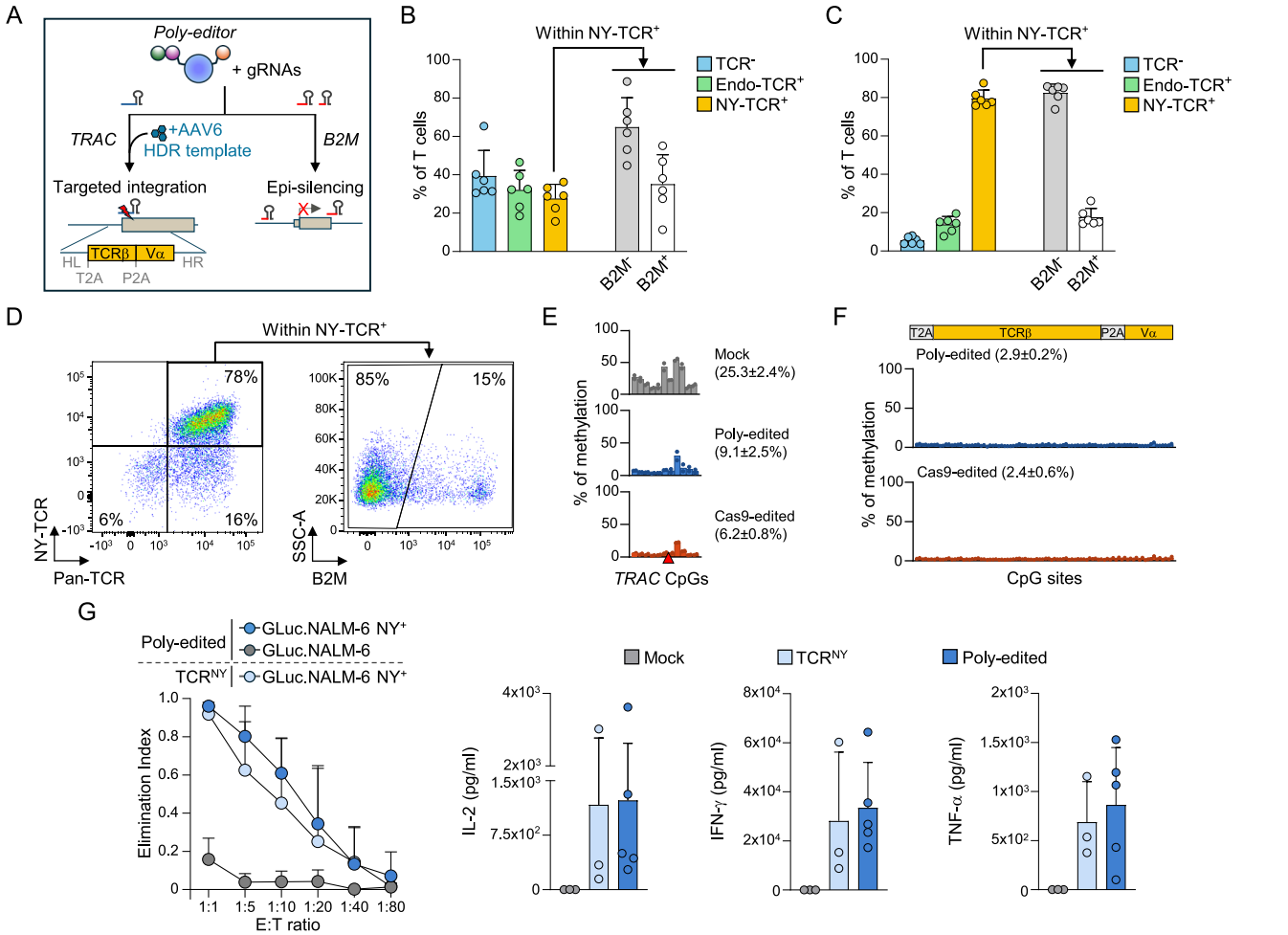

Fig. 6 | Polyfunctional editing mediates TCR replacement and *B2M* epi-silencing in T cells. A Polyfunctional editing strategy used to epi-silence *B2M* and insert the NY-ESO-1-specific TCR into *TRAC*. TCRβ: beta chain of the NY-ESO-1 TCR. Vα: variable region of the NY-ESO-1 TCR alpha chain. T2A and P2A: 2A self-cleaving peptides from *Thosea asigna virus* and *Porcine teschovirus-1*, respectively. **B** Percentages of the indicated T cell populations as measured by flow cytometry 31 days after poly-editing (mean ± SD of 6 blood donors). TCR$^-$: TCR-negative cells (light blue bar). Endo-TCR$^+$: cells positive for the endogenous TCRs (light green bar). NY-TCR$^+$: NY-ESO-1 TCR-positive cells (ochre bar). B2M$^-$: B2M-negative cells (gray bar). B2M$^+$: B2M-positive cells (white bar). **C** Percentages of the indicated T cell populations as measured by flow cytometry 13 days after poly-editing with the Alt-R™ HDR Enhancer V2 (mean ± SD of 6 blood donors). Bars are colored as indicated in (**B**). **D** Representative flow cytometry dot plots of poly-edited T cells from (**C**) showing expression of the TCRs (left plot), including the NY-ESO-1-specific one, and B2M (right plot), the latter gated on the double-positive cells. **E**, **F** CpG methylation profiles across the *TRAC* locus (panel **E**; Chr.14: 22,547,262-22,548,007) and the NY-ESO-1 TCR cassette (panel **F**) in the indicated T cell populations (mean ± SD of 2 blood donors). Mean methylation levels are in brackets. Red triangle: *TRAC* gRNA target site. **G** Left: anti-tumor activity, expressed as elimination index, of the indicated T cell populations cultured for 96 h with GLuc.NALM-6 expressing (NY$^+$; dark or light blue dots) or not (gray dots) NY-ESO-1 (mean ± SD of 3 blood donors for Mock and TCR^{NY}, and 5 blood donors for Poly-edited cells). TCR^{NY}: T cells engineered solely by targeted insertion of the NY-ESO-1 TCR into *TRAC*. Right: cytokine profiles of Mock-treated (gray bars), TCR^{NY} (light blue bars), and poly-edited (dark blue bars) T cells after 96 h of co-culture with GLuc.NALM-6 NY$^+$ cells at a 1:10 ratio. E:T: ratio between effector T cells and target cells. IFN-γ: interferon-gamma. IL-2: interleukin-2. TNF-α: tumor necrosis factor-alpha. No statistically significant differences were detected by one-way ANOVA with Tukey's multiple comparisons test. Graphs were generated using GraphPad Prism (GraphPad Software). Source data are provided as a Source Data file.

by the DNA repair processes[51], rather than by the epigenetic activity of the poly-editor.

To demonstrate the engineering potential of the platform, we (i) directed insertion of an autonomous transgene expression cassette into a safe harbor site, (ii) replaced the endogenous T cell specificity with a new one, (iii) inactivated the endogenous TCR by inserting a prototypic CAR and a selectable marker, or (iv) knocked into a ubiquitously expressed gene a CAR and an immunomodulatory receptor. For all approaches, we concurrently silenced one or two genes of potential clinical relevance for cancer immunotherapy. Among the proposed engineering modules, the most versatile is likely the final one, in which T cells are armed with a CAR and programmed to escape - at least in part - host immune surveillance through the simultaneous inactivation of polymorphic HLAs and ectopic expression of scHLA-E. Furthermore, these cells are incapable of attacking the host and resistant to the immunosuppressive effects of TGF-β because they lack surface expression of cognate receptors. This module could be further refined, for example, by replacing or expanding the panel of silenced genes, or by introducing additional payloads to enhance both anti-tumor efficacy[8] and the immune-evasive capacity of the engineered cells[52,53], thereby fine-tuning the cellular profile to specific tumor types. Importantly, all these polyfunctional procedures did not impair T cell function, as shown by cytotoxic activity and release of pro-inflammatory cytokines upon encounter with tumor target cells both in vitro and in vivo. While showcased here for T cells, we anticipate that polyfunctional editing could be readily applicable to other indications requiring sophisticated multiplexed cell engineering. In this context, it will be interesting to assess whether the polyfunctional editing

https://doi.org/10.1038/s41467-026-72846-2

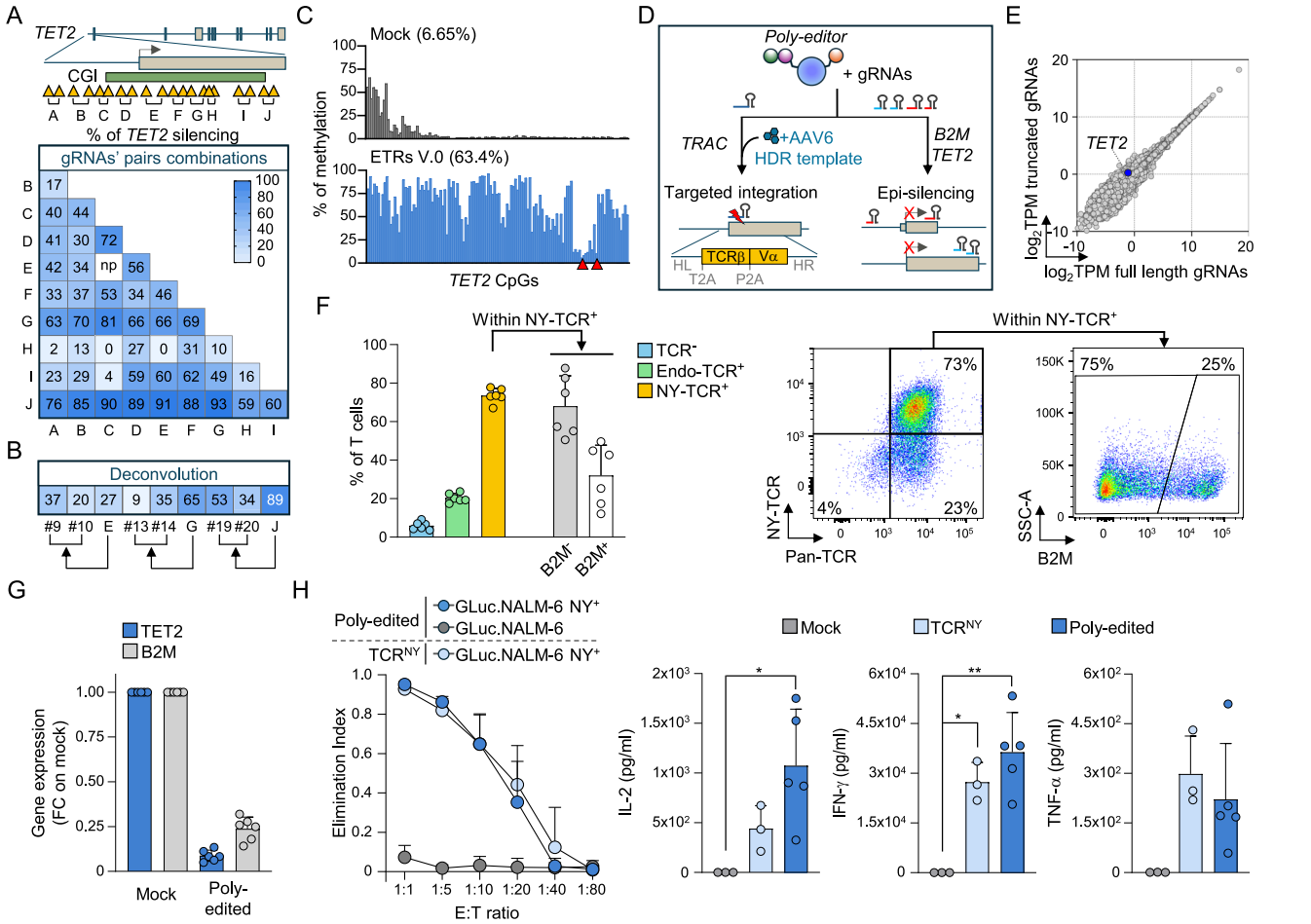

Fig. 7 | Polyfunctional editing supports multiplexed epi-silencing. A Top: to-scale schematic of the *TET2* promoter region showing the target sites of the ten tested gRNA pairs (letters from A to J; yellow triangles). Bottom: percentage of *TET2* epi-silencing at day 28 post-transfection with the indicated gRNA pairs and mRNAs encoding the triple ETR combination V.0. Data were normalized to *TET2* expression levels in mock-treated T cells. np: not performed. **B** Percentage of reduction in *TET2* expression for the indicated gRNA pairs and the corresponding single gRNAs. **C** CpG methylation profiles across the *TET2* promoter region (Chr. 4: 105,145,588-105,147,401) of mock-treated and epi-silenced T cells, with mean methylation levels indicated in brackets. Red triangles: *TET2* gRNA target sites. **D** Polyfunctional editing strategy used to epi-silence *B2M* and *TET2* and to insert the NY-ESO-1 TCR into exon 1 of *TRAC*. **E** Scatter plot comparing whole-transcriptome analyses of T cells treated with the tripartite ETR and either full-length or truncated *TET2* gRNAs ($n = 2$ experimental replicates). Data are expressed as $\log_2$ of TPM of mapped reads. **F** Left: percentages of the indicated T cell populations as measured by flow cytometry 13 days after polyfunctional editing (mean ± SD of 6 blood donors). Sample labeling as defined in Fig. 6B. Right: representative flow cytometry dot plots of poly-edited cells analyzed as in Fig. 6D. **G** Fold-change in *TET2* (blue bars) and *B2M* (gray bars) expression in poly-edited cells relative to mock-treated cells (mean ± SD of 6 blood donors). **H** Left: elimination index of the indicated T cell populations cultured for 96 h with GLuc.NALM-6 expressing (NY^+; dark or light blue dots) or not (gray dots) NY-ESO-1 (mean ± SD of 3 blood donors for Mock and TCR^{NY}, and 5 blood donors for Poly-edited T cells). Right: cytokine profiles of Mock-treated (gray bars), TCR^{NY} (light blue bars), and poly-edited (dark blue bars) T cells after 96 h of co-culture with GLuc.NALM-6 NY^+ cells at a 1:10 E:T ratio. $^*p = 0.0192$ (IL-2), $^*p = 0.0138$ (IFN-γ), $^{**}p = 0.0013$ by one-way ANOVA with Tukey's multiple comparisons test. Graphs were generated using GraphPad Prism (GraphPad Software). Source data are provided as a Source Data file.

strategy described here is compatible with other Cas9 orthologs, including more compact variants that may better fit with viral and non-viral in vivo delivery methods.

Polyfunctional editing, exploiting a single-editor design, can be executed in a single step, streamlining the manufacturing process and reducing the costs and potential toxicities associated with the simultaneous or sequential use of orthogonal or homologous editors[13,35,50,54], respectively. Furthermore, it delivers editing efficiencies that are almost comparable to those obtained with individual editing technologies. Although epi-silencing in T cells was slightly reduced when using truncated gRNAs, this approach remains compatible with current manufacturing processes that typically involve one or more steps of enrichment for the cells harboring the desired antigen-specificity. Editing efficiencies could be further increased by acting independently on the two activities of the platform. Regarding HDR-mediated transgene insertion, one may exploit alternative donor DNA formats and delivery modalities[55]. For epi-silencing, incorporating additional guides, selecting more efficient gRNA combinations from broader screenings, and/or adopting more powerful editors' designs could be considered. Of note, our optimization efforts yielded an improved architecture that outperformed its parental designs across all tested genes and cell types, including T cells. These studies also revealed general principles for improved ETR design. Specifically, we found that positioning the effector domains at the N-terminus of dCas9, along with a glycine-rich linker, proved beneficial for the ETR combinations. Conversely, the all-in-one architectures benefitted from positioning the DNA methyltransferase activity and the KRAB domain at the C- and N-terminus of dCas9, respectively, along with XTEN linkers. These improved designs may serve as blueprints for further ETR optimizations, which may foresee incorporating new effector domains identified from large-scale screenings[56,57].

https://doi.org/10.1038/s41467-026-72846-2

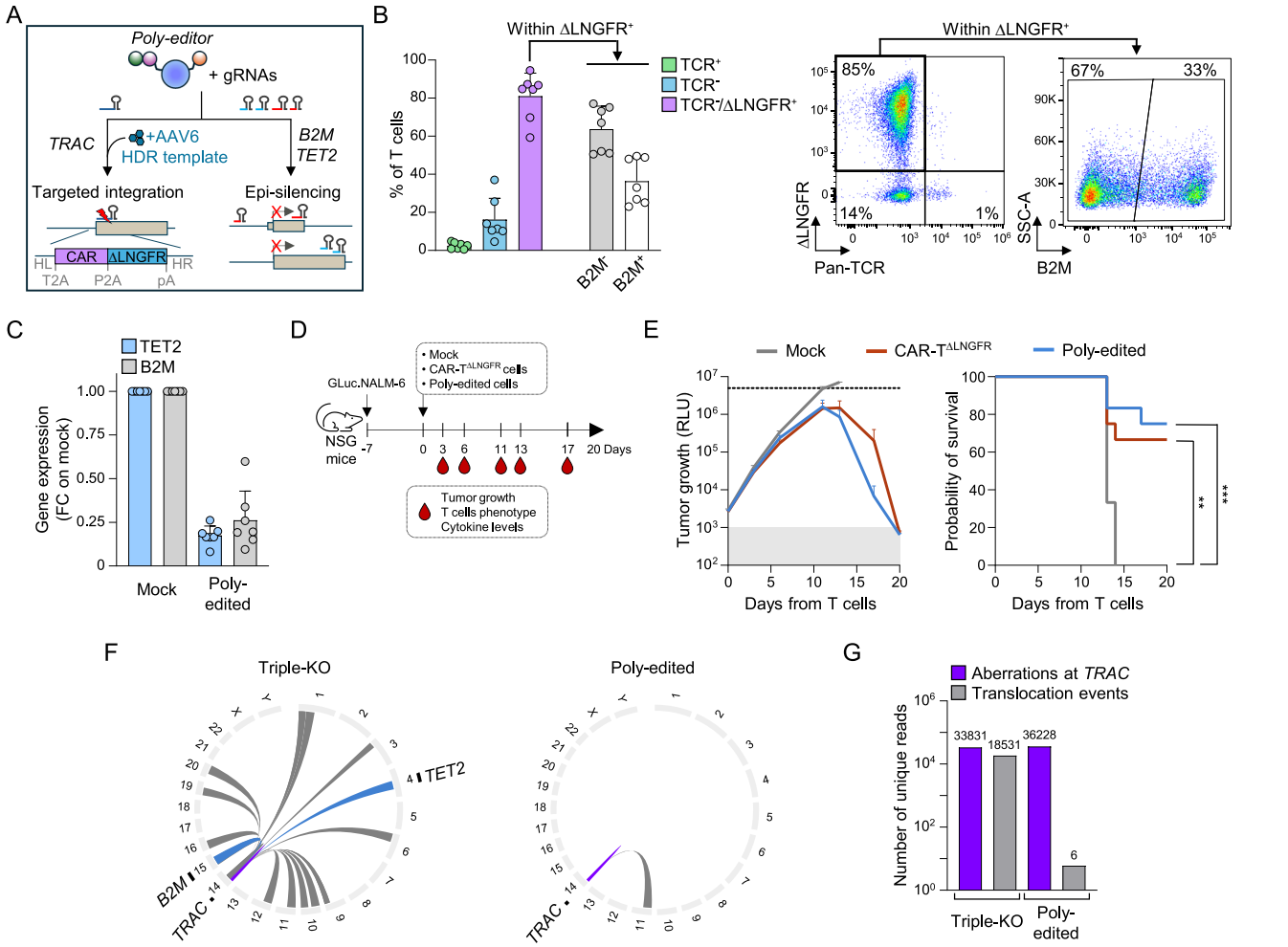

Fig. 8 | Polyfunctional editing for CAR-T cell engineering. A Polyfunctional editing strategy for the epi-silencing of *B2M* and *TET2* and insertion of the CD19–28ζ CAR:ΔLNGFR construct into *TRAC*. **B** Left: percentages of the indicated T cell populations at day 14 after poly-editing (mean ± SD of 7 blood donors). TCR$^+$: TCR-positive cells (green bar). TCR$^-$: TCR-negative cells (light blue bar). TCR$^-$/ΔLNGFR$^+$: cells negative for endogenous TCRs and positive for ΔLNGFR (lilac bar). B2M$^-$: B2M-negative cells (gray bar). B2M$^+$: B2M-positive cells (white bar). Right: representative flow cytometry dot plots of poly-edited T cells showing expression of the TCRs and ΔLNGFR (left plot) and, within the TCR$^-$/ΔLNGFR$^+$ cells, of B2M (right plot). **C** Fold-change in *TET2* (light blue bars) and *B2M* (gray bars) expression in poly-edited *vs.* mock-treated cells (mean ± SD of 7 blood donors). **D** Schematic of the in vivo experiment. NSG mice were injected with GLuc.NALM-6 cells and, 7 days later, with the indicated T cell populations. Peripheral blood was collected at the indicated time points to measure tumor growth, phenotype human T cells, and quantify cytokine release. Mock: mock-transfected T cells. CAR-T$^{\Delta LNGFR}$: T cells expressing CD19–28ζ CAR:ΔLNGFR from *TRAC*. Poly-edited cells: T cells expressing CD19–28ζ CAR:ΔLNGFR from *TRAC* with epi-silencing of *B2M* and *TET2*. **E** Tumor growth (left; mean ± SEM) and survival (right) curves over 20 days post-transplantation of the indicated T cell populations. $n = 6$ mice for Mock; $n = 12$ mice for each other group. $^{**}p = 0.0075$, $^{***}p = 0.0008$ by Mantel-Cox (log-rank) test. **F** Circos plots from CAST-Seq analyses of triple KO (left) and poly-edited (right) T cells ($n = 2$ experimental replicates). Triple-KO cells were transfected with mRNA encoding Cas9 and the *TRAC* gRNA, together with gRNA$^{B\#6}$ and gRNA$^{TE\#19}$. For poly-editing, the *TRAC* gRNA and the selected guide combinations for *B2M* and *TET2* were used. Aberrations at the *TRAC* locus are in violet; translocations between *TRAC* and either *B2M* or *TET2* are in blue; translocations between *TRAC* and OT sites of all gRNAs are in gray. **G** Number of unique CAST-Seq reads corresponding to either aberrations (violet bars) or translocations (gray bars) at the *TRAC* locus in the indicated treatments. Graphs were generated using GraphPad Prism (GraphPad Software). Source data are provided as a Source Data file.

Notably, epi-silencing proved to be effective also in this highly proliferating cell type, as also shown in previous studies[23,35,36,58]. In this context, the epigenetic changes induced by the editor are remarkably stable, withstanding the multiple rounds of cell division and metabolic reactivation associated with artificial or antigen-specific T-cell restimulations. Furthermore, two interesting findings emerged from our studies, which might be relevant for the future development of this platform. First, poly-editing retains high epi-silencing efficiency across diverse guide truncations. While this result may raise safety concerns related to the fact that shorter gRNAs may have more off-target sites in the genome, our transcriptional analyses indicate that truncated and full-length guides have comparable specificity profiles. Therefore, truncated guides may represent a valid alternative to full-length gRNAs also for safe epi-silencing. Secondly, gRNA combination results in higher epi-silencing efficiency, highlighting a simple yet effective strategy to enhance or even enable epigenetic silencing of genes that poorly respond to single-guide treatment. Our data uncover predicted and unpredicted effects of this strategy, where gRNA combination resulted in either additive or synergistic effects. Further studies are required to understand the rules determining the higher efficiency of multi *vs.* single-site targeting approaches for precise gene regulation.

In terms of safety, polyfunctional editing stands out from current T-cell engineering approaches operating through multiple DNA breaks, including multiple orthogonal gene editors[13] or combinations of base editors and orthogonal gene editors[50,54]. Indeed, it abrogates the risk of reciprocal chromosomal translocations among the edited genes, as only one of these genes undergoes editing through a

https://doi.org/10.1038/s41467-026-72846-2

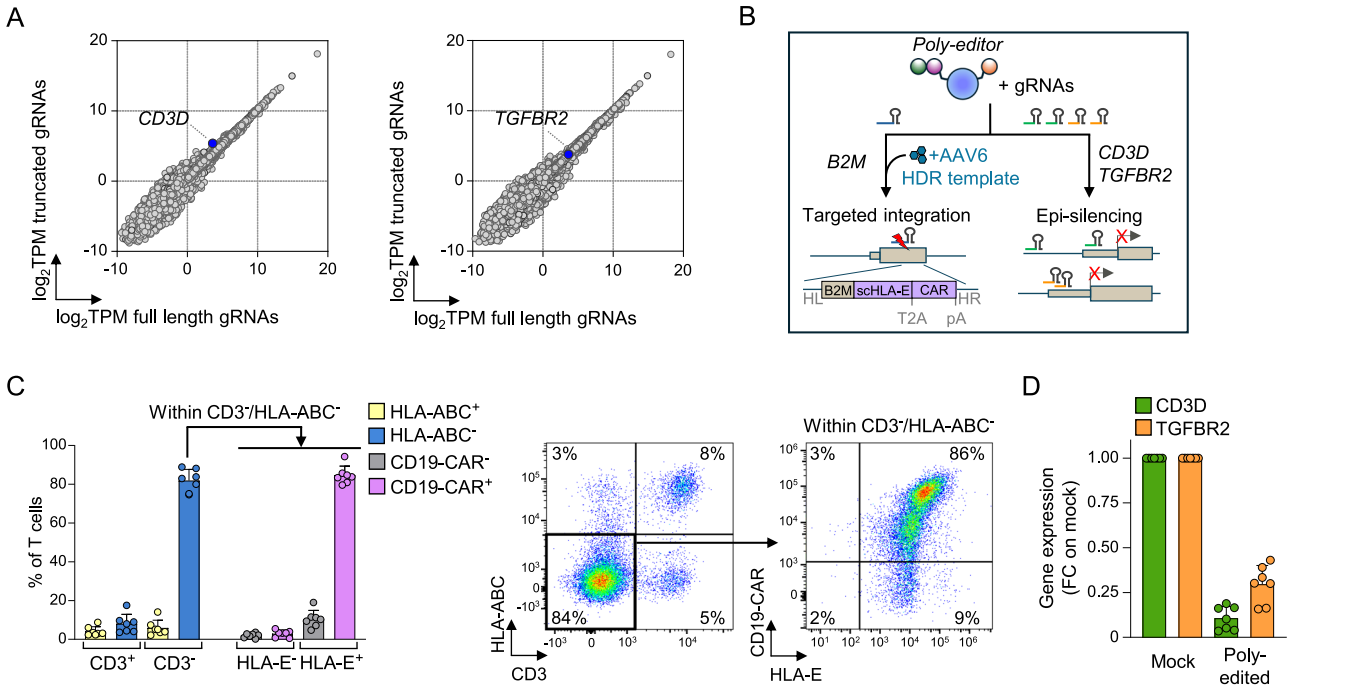

Fig. 9 | Generation of hypo-immune CAR-T cells through polyfunctional editing. A Scatter plot comparing whole-transcriptome analyses of T cells treated with the tripartite ETR and either full-length or truncated gRNAs targeting *CD3D* (left) or *TGFBR2* (right) ($n = 2$ experimental replicates). Data are expressed as log_2 TPM of mapped reads. **B** Polyfunctional editing strategy used to epi-silence *CD3D* and *TGFBR2* and insert the scHLA-E:CD19–28ζ CAR cassette into exon 1 of *B2M*. **C** Left: percentages of the indicated T cell populations as measured by flow cytometry 14 days after polyfunctional editing (mean ± SD of 7 blood donors). HLA-ABC$^+$: HLA-ABC-positive cells (light yellow bars); HLA-ABC$^-$: HLA-ABC-negative cells (blue bars); CD19-CAR$^-$: cells negative for the expression of the CD19–28ζ CAR (gray bars); CD19-CAR$^+$: cells positive for the expression of the CD19–28ζ CAR (lilac bars); CD3$^+$: CD3-positive cells; CD3$^-$: CD3-negative cells; HLA-E$^-$: HLA-E-negative cells; HLA-E$^+$: HLA-E-positive cells. Right: representative flow cytometry dot plots of poly-edited T cells showing the expression levels of the HLA-ABC and CD3 (left plot) and, within the double-negative cells, of HLA-E and CD19-CAR (right plot). **D** Fold-change in the expression levels of *CD3D* (green bars) and *TGFBR2* (orange bars) in poly-edited cells relative to mock-treated cells, 14 days post-editing (mean ± SD of 7 blood donors). Graphs were generated using GraphPad Prism (GraphPad Software). Source data are provided as a Source Data file.

mechanism involving DNA cleavage, while the others are transcriptionally silenced via epigenetic regulation. However, in its current configuration, polyfunctional editing cannot prevent translocations between the gene cleaved by Cas9 and potential off-target sites of its gRNA, nor can it avoid on-target genomic aberrations, which are emerging as frequent byproducts of DSB repair[9,10]. The former risk could be mitigated by adopting guides with a high specificity profile, high-fidelity Cas variants[59], and/or by incorporating an exonuclease within the editor[15]. On-target genomic aberrations could be reduced by using pharmacological interventions that promote HDR over NHEJ[60] or by exploiting Cas9 nickases that, through the activation of the DDR, can still promote targeted transgene insertion[61], although at lower levels than standard Cas9.

In conclusion, we establish proof-of-principle for polyfunctional editing in primary T cells using a single-molecule editor. This strategy has the potential to enhance safety, reduce costs, and increase anti-tumor potency, while enabling sophisticated genome and epigenome engineering in a single step.

Methods

Ethics statement

Buffy coats from healthy donors were obtained as anonymized residues of blood donations at the San Raffaele Hospital (Milan, IT) and were used upon signature of specific institutional informed consent for blood product donation. The experimental procedures involving human T cells were authorized by the San Raffaele Scientific Institutional Ethical Committee (protocol TIGET09). The experimental procedures involving mice were approved by the Institutional Animal Care and Use Committee (IACUC) and authorized by the Italian Ministry of Health and local authorities according to Italian law.

Cell culture conditions

HEK 293T (CRL-3216, ATCC) cells were cultured in IMDM (Gibco), while K-562 cells (CCL-243 ATCC), B2M^{tdTomato} K-562 cells[23], Jurkat clone E6-1 (TIB-152, ATCC) and GLuc.NALM-6 cells[41], either expressing or not expressing NY-ESO-1, were maintained in RPMI-1640 (Sigma-Aldrich). All media were supplemented with 10% Fetal Bovine Serum (FBS, EuroClone), 1% L-glutamine (Euroclone), and 1% penicillin/streptomycin (Euroclone). Cells were cultured at 37 °C in 5% CO_2. Primary human T lymphocytes were isolated from buffy coat-derived Peripheral Blood Mononuclear Cells (PBMCs) of healthy donors by Lympholyte®H (Cedarlane) density gradient centrifugation, followed by CD3-positive purification using Pan T cells isolation kit (Miltenyi Biotech). Purity was assessed by flow cytometry (BD FACSCanto™ II, BD Biosciences) using anti-CD3 (317318, BioLegend), anti-CD8 (344708, BD Biosciences), and anti-CD4 (317429, BioLegend) antibodies. T cells were activated for 48 h using anti-CD3/CD28 Dynabeads (Thermo Fisher Scientific) at a 1:1 ratio and cultured at 1.5×10^6 cells/ml in RPMI supplemented with 1% penicillin/streptomycin, 2% L-glutamine, 10% FBS and 5 ng/ml of each IL-7 and IL-15 (PeproTech) at 37 °C in 5% CO_2. When cultured long-term in vitro, T cells were restimulated for 48h with anti-CD3/CD28 Dynabeads at a 1:1 ratio or, in the case of CD3 epi-silenced cells, for 5h with 5ng/ml phorbol 12-myristate 13-acetate (PMA; Sigma-Aldrich) and 500ng/ml Ionomycin (Sigma-Aldrich).

https://doi.org/10.1038/s41467-026-72846-2

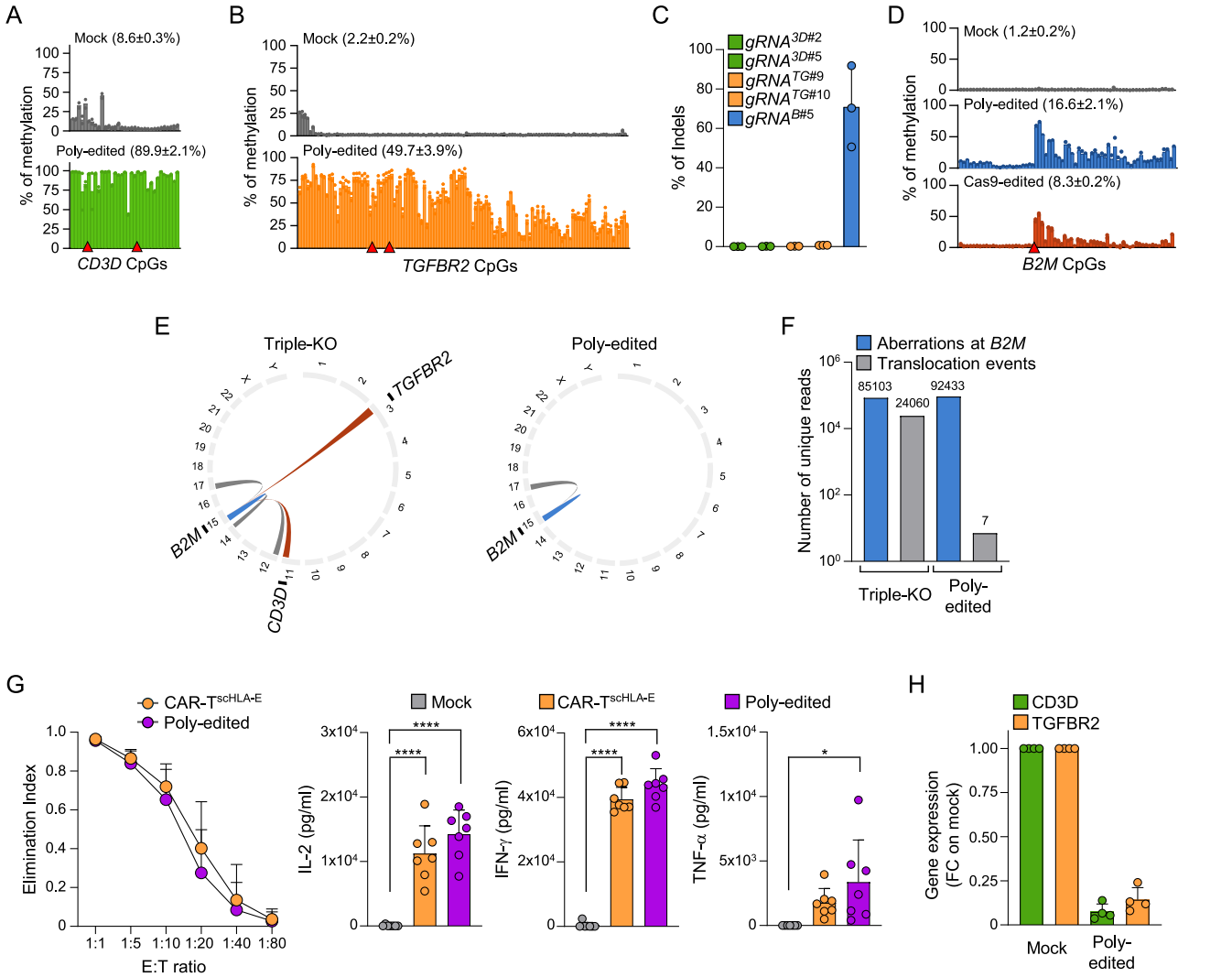

Fig. 10 | Molecular and functional characterization of poly-edited hypo-immune CAR-T cells. A, **B** CpG methylation profiles across *CD3D* (panel **A**; Chr.11: 118,341,599-118,343,630) and *TGFBR2* (panel **B**; Chr.3: 30,606,048-30,607,757) of mock-treated and poly-edited T cells (mean ± SD of 2 blood donors), with mean methylation levels indicated in brackets. Red triangles: gRNA target sites. **C** Percentages of indels of the *CD3D* (green bars), *TGFBR2* (orange bars), and *B2M* (blue bar) gRNAs in poly-edited cells (mean ± SD of 3 blood donors). **D** CpG methylation profiles across the *B2M* promoter in mock-treated, poly-edited, and Cas9-edited T cells (mean ± SD of 2 blood donors), with mean methylation levels indicated in brackets. Red triangle: *B2M* gRNA$^{B\#5}$ target site. **E** Circos plots from CAST-Seq analyses of triple-KO (left) and poly-edited (right) T cells ($n = 2$ experimental replicates). Triple-KO cells were transfected with mRNA encoding Cas9 and gRNA$^{B\#5}$ together with gRNA$^{3D\#5}$ and gRNA$^{TG\#9}$. For poly-editing, the gRNA$^{B\#5}$ and the selected guide combinations for *CD3D* and *TGFBR2* were used. Aberrations at the *B2M* locus are indicated in blue, translocations between *B2M* and either *CD3D* or *TGFBR2* in red, and translocations between *B2M* and OT sites of the *CD3D* or *TGFBR2* gRNAs in gray. **F** Bar plot showing the number of unique CAST-Seq reads corresponding to either aberrations (blue bars) or translocations (gray bars) at the *B2M* locus in the indicated treatments. **G** Left: elimination index of poly-edited (purple dots) and CAR-T$^{scHLA-E}$ (orange dots) cells cultured for 96 h with GLuc.NALM-6 (mean ± SD of 7 blood donors). Right: cytokine profiles of Mock-treated (gray bars), CAR-T$^{scHLA-E}$ (orange bars), and poly-edited (purple bars) T cells after 96 h of co-culture with GLuc.NALM-6 at a 1:10 E:T ratio. *$p = 0.0143$, ****$p < 0.0001$ by one-way ANOVA with Tukey's multiple comparisons test. **H** Fold-change in *CD3D* (green bars) and *TGFBR2* (orange bars) expression between mock-treated and poly-edited T cells after killing of the leukemia (mean ± SD of 4 blood donors). Graphs were generated using GraphPad Prism (GraphPad Software). Source data are provided as a Source Data file.

Molecular cloning and mRNA production

Cas9, ETRs, poly-editors and gRNAs were cloned into previously described mammalian expression plasmids[25]. Modified mRNAs were generated by in vitro transcription using the T7 Megascript Kit (Thermo Fisher Scientific), incorporating CleanCap-AG (4 mM; Trilink BioTechnologies) and substituting UTPs with N1-Met-ψ-Uridine (7.5 mM; Trilink BioTechnologies). mRNAs were purified using the RNeasy Mini Kit (Qiagen), quantified by NanoDrop 8000 (Thermo Fisher Scientific) and assessed for integrity using a 4200 TapeStation System. gRNAs targeting the human *B2M*, *TET2*, *CD3D*, and *TGFBR2* were designed using CHOPCHOP and selected among the top-ranking guides. gRNAs targeting *CD151* and *CD81* were previously described[24]. All gRNAs were synthesized by IDT according to a previously described nucleotide-modification scheme[62]. gRNAs targeting *AAVS1* and *TRAC*, as well as associated AAV6 donor templates, were adapted from published strategies[5,37]. The CD19-28ζ CAR:ΔLNGFR and the scHLA-E:CD19-28ζ-CAR HDR donor templates were designed in silico and then synthesized and cloned into an AAV transfer plasmid backbone by GenScript. AAV6 vectors were produced by InnovAAVector. The sequences of the ETRs, gRNAs, and HDR donor templates used in this study are present in Supplementary Data 2, 3, 4 respectively. The plasmids used in this study are available upon signing of a material transfer agreement.

Cell engineering procedures

GLuc.NALM-6 NY$^+$ were generated by transducing GLuc.NALM-6 cells with a bidirectional lentiviral vector[63] encoding NY-ESO-1 and the puromycin resistance gene. Transduced cells were selected for 10 days with puromycin (2 µg/ml; Sigma-Aldrich), and NY-ESO-1 expression was confirmed by qPCR analysis. For the editing experiments in cell lines, 5×10^5 cells were transfected using the Lonza 4D-Nucleofector™ system with either 2 µg of total plasmid DNA (and 3 µg of plasmid HDR template, when required) or 1.5 µg of total mRNA, maintaining a constant 1:1 editor-to-gRNA weight ratio in all conditions. Nucleofections were performed in the SF Cell Line solution for K-562, *B2M*^{dTomato} K-562 (FF-120 pulse program), and HEK 293T (CM-130 program) or in P3 Primary Cell solution for Jurkat (CL-120 program). Cells were then plated in U-bottom 96-well plates in complete medium. For the in vitro editing experiments in primary human T cells, two days after activation and following Dynabeads removal, $5{\times}10^5$ cells were nucleofected using the Lonza 4D-Nucleofector™ system (P3 Primary Cell solution, EO-115 program) with 1.5 µg of mRNA encoding the indicated editors and 3 µg of each epi-silencing gRNA and/or 1 µg of each gene targeting gRNA. T cells nucleofected with Phosphate-Buffered Saline (PBS) were used as mock-treated controls. Immediately after nucleofection, 80 µl of RPMI was added directly to the cuvette and cells were incubated for 15 min at 37 °C and then transferred to U-bottom 96-well plates containing 100µl of pre-warmed 2X medium (RPMI supplemented with 20% FBS, 4 mM L-Glutamine, 2% P/S, and 10 ng/ml each of IL-7 and IL-15). Immediately after plating, cells were transduced with the AAV6 vector containing the HDR donor template at a multiplicity of infection (MOI) of 1×10^5 and, where indicated, treated with 1µM Alt-R™ HDR Enhancer V2 (IDT). For the in vivo experiment, 1.5×10^7 T cells were transfected with 7.5 µg of mRNA of the poly-editor and 15 µg for each gRNA, or with PBS (mock-treated cells) in Opti-MEM (Gibco) using the MaxCyte GTx system and OC100x2 cuvettes with the expanded protocol T3. Following transfection, cells were incubated for 15 min at room temperature and then transferred to 6-well plates containing 6 ml of pre-warmed media (RPMI supplemented with 10% FBS, 2 mM L-Glutamine, 1% P/S, and 5 ng/mL each of IL-7 and IL-15). Cells were subsequently treated with 1µM Alt-R™ HDR Enhancer V2 and transduced with CD19-28ζ CAR:ΔLNGFR AAV6 vector at an MOI of 1×10^5. Three to six days later, cells were transferred to G-Rex6 well plates (Wilson Wolf) and expanded for an additional 7-10 days prior to cryopreservation.

Flow cytometry and cell sorting

Flow cytometry analyses were performed using BD FACSCanto™ II (BD Biosciences) or CytoFLEX S (Beckman Coulter), and raw data were analyzed using FlowJo v10.10.0 software. To assess editing efficiencies in vitro, cells were stained with conjugated antibodies against human B2M (316312, BioLegend), α/β TCR (306722, BioLegend), TCR Vβ13.1 (IM1554, Beckman Coulter), CD151 (350408, BioLegend), CD81 (349516, BioLegend), CD271 (a.k.a. LNGFR; 130-113-422, Miltenyi), CD3 (345763, BD Biosciences), HLA-ABC (565332, BD Biosciences), HLA-E (130-117-402, Miltenyi), and CD19 CAR FMC63 Idiotype (130-127-342, Miltenyi). Cell sorting was carried out on the BD FACSAria™ Fusion (BD Biosciences). To profile human T cells in vivo, cells were stained with conjugated antibodies against human CD45 (304036, BioLegend), CD4 (345770, BD Biosciences), CD271 (557196, BD Biosciences), HLA-DR (307618, BioLegend), PD-1 (329918, BioLegend), CD45RA (304106, BioLegend), and CD62L (304826, BioLegend) and acquired together with Flow Cytometry Counting Beads (Beckman Coulter) to assess T-cell absolute count.

T cell functional assays

To assess functional activity of T cells in vitro, cells were co-cultured with the GLuc.NALM-6 cell line[41] expressing or not NY-ESO-1 at the indicated Effector-to-:Target (E:T) ratios. Mock-treated T cells were used as controls. After four days of co-culture, supernatants were collected and analyzed with the LEGENDplex™ beads-based cytokine immunoassay (BioLegend) according to manufacturer's instructions. GLuc-derived bioluminescence, obtained using the QUANTI-Luc™ 4 Lucia/Gaussia kit (InvivoGen), was measured with the Mithras Multimode Reader (Berthold Technologies) and expressed as Relative Luminescence Units (RLU). Tumor cell killing was expressed as an elimination index and calculated with the following formula:

$$1 - \left(\frac{\mathrm{RLU}_{\text{target cells + tumor-specific T cells}}}{\mathrm{RLU}_{\text{target cells + mock-treated T cells}}} \right)$$

To assess functional activity of T cells in vivo, male and female eight-week-old NOD-scid IL2rg$^{-/-}$ (NSG) mice (Charles River Laboratories) were intravenously (i.v.) injected with 0.5×10^6 GLuc.NALM-6 cells. Seven days later, mice were treated i.v. with 3.5×10^6 poly-edited CAR-T cells, control-edited CAR-T$^{\Delta LNGFR}$ cells, or Mock T cells. Tumor burden was monitored by measuring RLU in the blood over time. Mice were randomized based on RLU values obtained on day 4 after leukemia injection to ensure comparable tumor distribution among treatment groups prior to T cell infusion. Peripheral blood samples were collected at the time points indicated in Fig. 8D to monitor circulating human T cells by flow cytometry. The concentration of human cytokines in the plasma was measured using the LEGENDplex bead-based cytokine immunoassay (BioLegend) according to the manufacturer's instructions. Mice were sacrificed when RLU exceeded the threshold of 5×10^6.

Reciprocal translocation PCR analyses

Genomic DNA (gDNA) was extracted from 3 to 5×10^5 cells using the Maxwell RSC Cultured Cells DNA Kit (Promega) according to the manufacturer's instructions. gDNA concentration and purity were assessed using a NanoDrop One spectrophotometer. PCR amplifications were performed using the GoTaq Hot Start Polymerase (Promega) and the primer pairs listed in Supplementary Data 5. Detection of reciprocal translocations between *B2M* and *AAVS1* loci was carried out by endpoint PCR followed by analysis on a 4200 TapeStation System (Agilent Technologies). For quantitative analysis, translocation events were measured by ddPCR using the QX200™ ddPCR™ EvaGreen Supermix (Bio-Rad) with 50 ng of gDNA and the same primer pairs mentioned above (Supplementary Data 5). Droplets were generated using an AutoDG Droplet Digital PCR System (Bio-Rad), PCR amplification was performed according to the manufacturer's instructions, and droplets were analyzed with the QX200 Droplet reader and QX Manager Software (Bio-Rad). The percentage of translocation events was calculated as the concentration of translocation relative to the reference gene *TERT*.

Transcriptional analyses

For gene expression analysis, total RNA was extracted from either 5×10^5 GLuc.NALM-6 cells or $3{-}5 \times 10^5$ T cells using RNeasy Micro Extraction Kit (Qiagen) according to the manufacturer's instructions. RNA was reverse transcribed using random hexamers with the SuperScript™ III First-Strand Synthesis SuperMix (Thermo Fisher Scientific). For NY-ESO-1 expression, quantitative real-time PCRs (qPCRs) were performed in triplicate using 20 ng of cDNA per reaction, Power SYBR™ Green PCR Master Mix (Applied Biosystems) and a ViiA 7 Real-Time PCR System (Applied Biosystems). Cycle threshold (Ct) values were extracted using the QuantStudio™ software (Applied Biosystems), and NY-ESO-1 expression was calculated relative to the reference gene *HPRT1* using the $2^{-\Delta Ct}$ method. For the expression of all other genes, ddPCR reactions were assembled with ddPCR Supermix for Probes (No dUTP, Bio-Rad) with 0.6 or 6 ng of cDNA and the following TaqMan assays (Thermo Fisher Scientific): *B2M* FAM HS00187842_m1, *GAPDH* VIC HS02758991_g1, *TET2* FAM Hs0032599_m1, *TGFBR2*

FAM HS00234253_m1, *CD3D* FAM Hs00174158_m1, *HPRT1* VIC Hs02800695_m1. Droplets were generated using an AutoDG Droplet Digital PCR System (Bio-Rad). PCR amplification was performed according to the manufacturer's instructions and analyzed with the QX200 Droplet reader and the QX Manager Software (Bio-Rad). Gene expression values normalized to the respective reference gene were expressed as fold change relative to mock-treated T cells. For whole transcriptomic analyses, total RNA was extracted from 10^6 cells using the RNeasy Mini Kit and quantified using the Qubit 2.0 Fluorimetric Assay (Thermo Fisher Scientific). For T cells, RNA was extracted 20 days after co-transfection with the tripartite ETR V.3 and either gene-specific gRNAs or an unrelated gRNA targeting the murine *Pcsk9* gene as a control (mock-treated). Stranded libraries were prepared with the NEBNext® Ultra™ II Directional RNA Library Prep Kit for Illumina after rRNA depletion, and sequencing was performed using an Illumina NovaSeq 6000 platform to obtain at least 30 M of 50 bp paired-end reads per sample. Read quality was controlled with Fastqc v0.11.16 (https://www.bioinformatics.babraham.ac.uk/projects/fastqc/), low-quality reads and adapter sequences were trimmed using Trim Galore v0.6.6 (https://www.bioinformatics.babraham.ac.uk/projects/trim_galore/) with the parameters --quality 20, --length 25, --paired. For $B2M^{tdTomato}$ K-562 samples, a custom reference was generated using the *reform* function (https://github.com/gencorefacility/reform) by inserting the tdTomato sequence into the *B2M* locus of the human GRCh38 reference genome and by adding a custom transcript containing the first exon of *B2M* fused to the tdTomato sequence to the Gencode v35 annotation (GENCODE - Human Release 35). High-quality reads were aligned to the custom reference genome using STAR v2.7.6a with default parameters, following a previously described approach[25]. For T cell samples, reads were aligned to the GRCh38 reference genome. To exclude contamination from epi-editor expressing vectors, reads were additionally aligned to the corresponding plasmid sequence and eventually removed from GRCh38-aligned BAM files. Gene counts were obtained using featureCounts (Subread v2.0.1) and read distribution modeled with DESeq2 v1.30.0. Differential gene expression analysis was performed using the nbinomWaldTest function, and p-values were corrected using the Benjamini-Hochberg (BH) method. Transcripts Per Million (TPM) values displayed in scatter plots were calculated using the length from the featureCounts output.

Targeted bisulfite sequencing

gDNA was extracted using the Maxwell RSC Cultured Cell extraction kit (Promega) and quantified using a NanoDrop 8000. Bisulfite DNA conversion was performed using the EpiTect Bisulfite kit (Qiagen) according to the manufacturer's instructions. Converted DNA was PCR-amplified using locus-specific primers (Supplementary Data 5) containing partial Illumina adapter sequences. A second round of PCR was performed to add full-length Illumina adapters and sample-specific barcodes. Libraries were sequenced using an Illumina MiSeq platform in a paired-end mode, generating 2 × 300 bp reads depending on the targeted genomic region. Read quality was controlled with Fastqc v0.11.9, and low-quality reads and adapter sequences were trimmed using Trim_Galore v0.6.6. with the parameters --quality 20, --length 25, --paired, --rrbs. For samples containing an integrated cassette, custom references were generated using the reform function (https://github.com/gencorefacility/reform) by inserting cassette sequences (i.e., PGK-GFP or NY-ESO-1 TCR) into the corresponding target gene within the GRCh38 human reference genome. High-quality reads were analyzed using the Bismark read mapper and Methylation caller tool v0.23.0[64]. Reads were aligned to both converted and unconverted versions of the reference genome using Bismark with the --local and the -X 600 parameters. Methylation calling was performed using the bismark_methylation_extractor script, selecting only those reads mapping to the original top or bottom strand based on the PCR primers. The methylation calls were loaded into the R environment and processed using the R/Bioconductor package methylKit v1.16.1[65]. Imported data were filtered to retain CpGs located within the selected genomic regions (and to remove errors) and normalized using the normalizeCoverage function. Data from different samples were merged using the unite function, considering the positions covered in at least one replicate per condition. The percentage of methylation at each CpG was calculated using the percMethylation function.

Indels quantifications

gDNA was extracted from 3 to 5×10^5 cells using the Maxwell RSC Cultured Cells DNA Kit (Promega) and PCR-amplified using the GoTaq Hot Start Polymerase (Promega) following manufacturer's instructions and primers listed in Supplementary Data 5. Gene editing efficiencies were evaluated by T7 endonuclease assay after amplification (Alt-R Genome Editing Detection Kit, IDT) according to the manufacturer's instructions. Alternatively, gDNA was PCR-amplified using locus-specific primers (Supplementary Data 5) containing partial Illumina adapter sequences. A second round of PCR was performed to add full-length Illumina adapters and sample-specific barcodes. Libraries were sequenced using an Illumina MiSeq platform in a paired-end mode, generating 2 × 250 bp reads. Reads were analyzed using CRISPResso2[66] to detect insertions and deletions. Since the amplicons were longer than the read length, reads were aligned using Bowtie2 (paired-end mode with default parameters) to a 300 bp region centered on the gRNA target site (± 150 bp). Original fastq files were subsetted to retain only reads mapping to the region of interest using the *filterbyname* module of the BBMap aligner (BBTools suite; sourceforge.net/projects/bbmap/). The retained reads were subsequently analyzed with CRISPResso2 in paired-end or single-end mode. Trimmomatic software (USADELLAB.org - Trimmomatic: A flexible read trimming tool for Illumina NGS data) was used to remove low-quality bases (score <30) and Illumina adapter sequences with the following options: --trim_sequences --trimmomatic_command trimmomatic --trimmomatic_options_string 'ILLUMINACLIP: TruSeq3-PE-2.fa:2:30:10 MINLEN:100'). Paired-end reads were first merged using FLASH to generate a single contig, which was then aligned to the corresponding input amplicon reference. For samples in which merging was not possible due to low second-mate quality, amplicon length, or gRNA position, reads were instead aligned directly in single-end mode and modifications were quantified accordingly. The gRNA sequences were provided to focus the analysis on the target regions, and the quantification window was defined as 20 bp on each side of the gRNA cut site. Identified alleles were quantified by measuring the number of reads and their relative abundance among total read counts, considering only insertions and deletions (Supplementary Data 6). Substitutions were excluded from the analysis, as they are likely attributable to PCR or sequencing errors.

CAST-Seq analyses

Poly-edited, triple-KO, or mock-treated T cells were generated by exposing them to Alt-R™ HDR Enhancer V2 in the absence of any donor DNA template. Then, 4 days post-nucleofection, gDNA was extracted using the DNeasy Blood and Tissue DNA Isolation Kit (Qiagen). Primer sequences used for CAST-Seq are listed in Supplementary Data 7. CAST-Seq analyses were performed as originally described[10], with a few modifications[67,68]. In brief, 500 ng of gDNA were used as input material for each technical replicate. Libraries were prepared using the NEBNext® Ultra™ II FS DNA Library Prep Kit for Illumina (NEB E7805L). Enzymatic fragmentation of the genomic DNA was aimed at an average length of 500–700 bp. CAST-Seq libraries were sequenced on a NovaSeq™ X Plus using 2 × 150 bp paired-end sequencing (GENEWIZ, Azenta Life Sciences). For each sample, 2 experimental replicates were run and analyzed. Only sites that were present in both experimental replicates and significant in two replicates are reported

(Supplementary Data 1). For sites under investigation, the spacer sequence of the gRNA was aligned to the most covered regions for each site (±400 bp)[67]. Sites were labeled as Off-Target (OT) if any of the two p-values reached the cutoff of 0.005[68]. The D-CAST-Seq bioinformatic pipeline for the simultaneous use of two gRNAs was used[68].

Statistics and reproducibility

Raw data were analyzed, and statistical significance was calculated using GraphPad Prism v.11.0.0 for Windows (GraphPad Software, Boston, MA, USA; www.graphpad.com). Statistical tests and significance are indicated in the figure legends. The number of replicates and whether they were biological or technical are indicated in the figure legends. Findings were reproducible across replicates. No statistical method was used to predetermine sample size. No data were excluded from the analyses. In vitro experiments were not randomized. For the in vivo experiment, mice were randomized according to leukemia burden, as determined by RLU values measured on day 4 following GLuc.NALM-6 injection, to ensure comparable tumor distribution among groups prior to T cell administration. The Investigators were not blinded to allocation during experiments and outcome assessment.

Reporting summary

Further information on research design is available in the Nature Portfolio Reporting Summary linked to this article.

Data availability

All data are available in the main text or the supplementary materials. The plasmids used in this study are available upon signing a Material Transfer Agreement (MTA). Data from RNA-seq, targeted bisulfite sequencing, targeted amplicon sequencing and CAST-Seq have been deposited on the Gene Expression Omnibus (GEO) database under accession number: GSE293143. Source data are provided with this paper.

References

1. Knott, G. J. & Doudna, J. A. CRISPR-Cas guides the future of genetic engineering. *Science* **361**, 866–869 (2018).
2. Jinek, M. et al. A programmable dual-RNA-guided DNA endonuclease in adaptive bacterial immunity. *Science* **337**, 816–821 (2012).
3. Mali, P. et al. RNA-guided human genome engineering via Cas9. *Science* **339**, 823–826 (2013).
4. Eyquem, J. et al. Targeting a CAR to the TRAC locus with CRISPR/Cas9 enhances tumour rejection. *Nature* **543**, 113–117 (2017).
5. Roth, T. L. et al. Reprogramming human T cell function and specificity with non-viral genome targeting. *Nature* **559**, 405–409 (2018).
6. Schober, K. et al. Orthotopic replacement of T-cell receptor α- and β-chains with preservation of near-physiological T-cell function. *Nat. Biomed. Eng.* **3**, 974–984 (2019).
7. Ruggiero, E. et al. CRISPR-based gene disruption and integration of high-avidity, WT1-specific T cell receptors improve antitumor T cell function. *Sci. Transl. Med.* **14**, eabg8027 (2022).
8. Bonini, C. et al. Genome editing in engineered T cells for cancer immunotherapy. *Hum. Gene Ther.* **34**, 853–869 (2023).
9. Kosicki, M., Tomberg, K. & Bradley, A. Repair of double-strand breaks induced by CRISPR-Cas9 leads to large deletions and complex rearrangements. *Nat. Biotechnol.* **36**, 765–771 (2018).
10. Turchiano, G. et al. Quantitative evaluation of chromosomal rearrangements in gene-edited human stem cells by CAST-Seq. *Cell Stem Cell* **28**, 1136–1147.e5 (2021).
11. Nahmad, A. D. et al. Frequent aneuploidy in primary human T cells after CRISPR-Cas9 cleavage. *Nat. Biotechnol.* **40**, 1807–1813 (2022).
12. Stadtmauer, E. A. et al. CRISPR-engineered T cells in patients with refractory cancer. *Science* **367**, eaba7365 (2020).
13. Bothmer, A. et al. Detection and modulation of DNA translocations during multi-gene genome editing in T. *Cells. CRISPR J.* **3**, 177–187 (2020).
14. Ottaviano, G. et al. Phase 1 clinical trial of CRISPR-engineered CAR19 universal T cells for treatment of children with refractory B cell leukemia. *Sci. Transl. Med.* **14**, eabq3010 (2022).
15. Yin, J. et al. Cas9 exo-endonuclease eliminates chromosomal translocations during genome editing. *Nat. Commun.* **13**, 1204 (2022).
16. Girardi, T., Vicente, C., Cools, J. & De Keersmaecker, K. The genetics and molecular biology of T-ALL. *Blood* **129**, 1113–1123 (2017).
17. Porto, E. M., Komor, A. C., Slaymaker, I. M. & Yeo, G. W. Base editing: advances and therapeutic opportunities. *Nat. Rev. Drug Discov.* **19**, 839–859 (2020).
18. Chiesa, R. et al. Base-edited CAR7 T cells for relapsed T-cell acute lymphoblastic leukemia. *N. Engl. J. Med.* **389**, 899–910 (2023).
19. Chiesa, R. et al. Universal base-edited CAR7 T cells for T-cell acute lymphoblastic leukemia. *N. Engl. J. Med.* **394**, 152–165 (2026).
20. Huang, M. E. et al. C-to-G editing generates double-strand breaks causing deletion, transversion and translocation. *Nat. Cell Biol.* **26**, 294–304 (2024).
21. Wu, L. et al. Adenine base editors induce off-target structure variations in mouse embryos and primary human T cells. *Genome Biol* **25**, 291 (2024).
22. Fiumara, M. et al. Genotoxic effects of base and prime editing in human hematopoietic stem cells. *Nat. Biotechnol.* **42**, 877–891 (2024).
23. Amabile, A. et al. Inheritable silencing of endogenous genes by hit-and-run targeted epigenetic editing. *Cell* **167**, 219–232.e14 (2016).
24. Núñez, J. K. et al. Genome-wide programmable transcriptional memory by CRISPR-based epigenome editing. *Cell* **184**, 2503–2519.e17 (2021).
25. Cappelluti, M. A. et al. Durable and efficient gene silencing in vivo by hit-and-run epigenome editing. *Nature* **627**, 416–423 (2024).
26. Tremblay, F. et al. A potent epigenetic editor targeting human PCSK9 for durable reduction of low-density lipoprotein cholesterol levels. *Nat. Med.* https://doi.org/10.1038/s41591-025-03508-x (2025).
27. Mao, S. et al. Design of optimized epigenetic regulators for durable gene silencing with application to PCSK9 in nonhuman primates. *Nat. Biotechnol.* https://doi.org/10.1038/s41587-025-02838-y (2025).
28. Fu, Y., Sander, J. D., Reyon, D., Cascio, V. M. & Joung, J. K. Improving CRISPR-Cas nuclease specificity using truncated guide RNAs. *Nat. Biotechnol.* **32**, 279–284 (2014).
29. Dahlman, J. E. et al. Orthogonal gene knockout and activation with a catalytically active Cas9 nuclease. *Nat. Biotechnol.* **33**, 1159–1161 (2015).
30. Kiani, S. et al. Cas9 gRNA engineering for genome editing, activation and repression. *Nat. Methods* **12**, 1051–1054 (2015).
31. Zhang, X. et al. MiniCAFE, a CRISPR/Cas9-based compact and potent transcriptional activator, elicits gene expression in vivo. *Nucleic Acids Res* **49**, 4171–4185 (2021).
32. Lombardo, A. et al. Site-specific integration and tailoring of cassette design for sustainable gene transfer. *Nat. Methods* **8**, 861–869 (2011).
33. Yi, Z. et al. Programmable DNA pyrimidine base editing via engineered uracil-DNA glycosylase. *Nat. Commun.* **15**, 6397 (2024).
34. Alerasool, N., Segal, D., Lee, H. & Taipale, M. An efficient KRAB domain for CRISPRi applications in human cells. *Nat. Methods* **17**, 1093–1096 (2020).
35. Goudy, L. et al. Integrated epigenetic and genetic programming of primary human T cells. *Nat. Biotechnol.* https://doi.org/10.1038/s41587-025-02856-w (2025).

36. Xu, D. et al. Programmable epigenome editing by transient delivery of CRISPR epigenome editor ribonucleoproteins. *Nat. Commun* **16**, 7948 (2025).
37. Vavassori, V. et al. Lipid nanoparticles allow efficient and harmless ex vivo gene editing of human hematopoietic cells. *Blood* **142**, 812–826 (2023).
38. Provasi, E. et al. Editing T cell specificity towards leukemia by zinc finger nucleases and lentiviral gene transfer. *Nat. Med.* **18**, 807–815 (2012).
39. Mastaglio, S. et al. NY-ESO-1 TCR single edited stem and central memory T cells to treat multiple myeloma without graft-versus-host disease. *Blood* **130**, 606–618 (2017).
40. Kagoya, Y. et al. Genetic ablation of HLA Class I, Class II, and the T-cell receptor enables allogeneic T cells to be used for adoptive T-cell therapy. *Cancer Immunol. Res.* **8**, 926–936 (2020).
41. Falcone, L. & Casucci, M. Exploiting secreted luciferases to monitor tumor progression in vivo. *Methods Mol. Biol.* **1393**, 105–111 (2016).
42. Fraietta, J. A. et al. Disruption of TET2 promotes the therapeutic efficacy of CD19-targeted T cells. *Nature* **558**, 307–312 (2018).
43. Dimitri, A. J. et al. TET2 regulates early and late transitions in exhausted CD8 + T cell differentiation and limits CAR T cell function. *Sci. Adv.* **10**, eadp9371 (2024).
44. Jo, S. et al. Endowing universal CAR T-cell with immune-evasive properties using TALEN gene editing. *Nat. Commun.* **13**, 3453 (2022).
45. Gornalusse, G. G. et al. HLA-E-expressing pluripotent stem cells escape allogeneic responses and lysis by NK cells. *Nat. Biotechnol.* **35**, 765–772 (2017).
46. Chimienti, R. et al. Engineering of immune checkpoints B7-H3 and CD155 enhances immune compatibility of MHC-I-/- iPSCs for β cell replacement. *Cell Rep.* **40**, 111423 (2022).
47. Kloss, C. C. et al. Dominant-negative TGF-β receptor enhances PSMA-targeted human CAR T cell proliferation and augments prostate cancer eradication. *Mol. Ther.* **26**, 1855–1866 (2018).
48. Tang, N. et al. TGF-β inhibition via CRISPR promotes the long-term efficacy of CAR T cells against solid tumors. *JCI Insight* **5**, e133977 (2020).
49. Fix, S. M. et al. CRISPR-mediated TGFBR2 knockout renders human ovarian cancer tumor-infiltrating lymphocytes resistant to TGF-β signaling. *J. Immunother. Cancer* **10**, e003750 (2022).
50. Murray, R. et al. Multiplex gene-editing strategy to engineer allogeneic EGFR-targeting CAR T-cells with improved efficacy against solid tumors. *Nat. Commun.* **16**, 11593 (2025).
51. Wang, M., Zhang, Y., Bi, C. & Li, M. CRISPR-Cas9-induced double-strand breaks disrupt maintenance of epigenetic information. *Genome Biol.* **26**, 411 (2025).
52. Hu, X. et al. Hypoimmune CD19 CAR T cells evade allorejection in patients with cancer and autoimmune disease. *Cell Stem Cell* **32**, 1356–1368.e4 (2025).
53. Deuse, T. & Schrepfer, S. Progress and challenges in developing allogeneic cell therapies. *Cell Stem Cell* **32**, 513–528 (2025).
54. Glaser, V. et al. Combining different CRISPR nucleases for simultaneous knock-in and base editing prevents translocations in multiplex-edited CAR T cells. *Genome Biol.* **24**, 89 (2023).
55. Shy, B. R. et al. High-yield genome engineering in primary cells using a hybrid ssDNA repair template and small-molecule cocktails. *Nat. Biotechnol.* **41**, 521–531 (2023).
56. Tycko, J. et al. High-throughput discovery and characterization of human transcriptional effectors. *Cell* **183**, 2020–2035.e16 (2020).
57. Tycko, J. et al. Development of compact transcriptional effectors using high-throughput measurements in diverse contexts. *Nat. Biotechnol.* https://doi.org/10.1038/s41587-024-02442-6 (2024).
58. Roman Azcona, M. S. et al. Sustained and specific multiplexed immune checkpoint modulation in CAR T cells induced by targeted epigenome editing. *Mol. Ther. Nucleic Acids* **36**, 102618 (2025).
59. Kleinstiver, B. P. et al. High-fidelity CRISPR-Cas9 nucleases with no detectable genome-wide off-target effects. *Nature* **529**, 490–495 (2016).
60. Wimberger, S. et al. Simultaneous inhibition of DNA-PK and Polϴ improves integration efficiency and precision of genome editing. *Nat. Commun.* **14**, 4761 (2023).
61. Ran, F. A. et al. Double nicking by RNA-guided CRISPR Cas9 for enhanced genome editing specificity. *Cell* **154**, 1380–1389 (2013).
62. Finn, J. D. et al. A single administration of CRISPR/Cas9 lipid nanoparticles achieves robust and persistent in vivo genome editing. *Cell Rep.* **22**, 2227–2235 (2018).
63. Amendola, M., Venneri, M. A., Biffi, A., Vigna, E. & Naldini, L. Coordinate dual-gene transgenesis by lentiviral vectors carrying synthetic bidirectional promoters. *Nat. Biotechnol.* **23**, 108–116 (2005).
64. Krueger, F. & Andrews, S. R. Bismark: a flexible aligner and methylation caller for Bisulfite-Seq applications. *Bioinformatics* **27**, 1571–1572 (2011).
65. Akalin, A. et al. methylKit: a comprehensive R package for the analysis of genome-wide DNA methylation profiles. *Genome Biol.* **13**, R87 (2012).
66. Clement, K. et al. CRISPResso2 provides accurate and rapid genome editing sequence analysis. *Nat. Biotechnol.* **37**, 224–226 (2019).
67. Rhiel, M. et al. T-CAST: an optimized CAST-Seq pipeline for TALEN confirms superior safety and efficacy of obligate-heterodimeric scaffolds. *Front. Genome Ed.* **5**, 1130736 (2023).
68. Klermund, J. et al. On- and off-target effects of paired CRISPR-Cas nickase in primary human cells. *Mol. Ther.* **32**, 1298–1310 (2024).

Acknowledgements

We thank the FRACTAL and the Genomics facilities of the IRCCS San Raffaele Scientific Institute for technical support, Alessio Cantore, and Samuele Ferrari for fruitful discussion. Rebecca Raab for technical assistance for CAST-Seq and Geoffroy Andrieux for analyzing CAST-Seq data (Medical Center—University of Freiburg, Freiburg, Germany). T.B. conducted this study as a partial fulfillment of her Ph.D. Funding. This study was supported by the European Research Council [Starting Grant no. 101076572] to M.Ca., Fondazione Telethon [SR-Tiget Core Grant no. TTALC1222TT] and Chroma Medicine Inc. to A.L.

Author contributions

Conceptualization: D.C., T.B., and A.L. Investigation: D.C., T.B., M.R., P.Q., A.R., R.E.K., M.A.C., S.A., V.M.P., and M.Co. Methodology: D.C., T.B., M.R., P.Q., A.R., R.E.K., M.A.C., and V.M.P. Data Curation: D.C., T.B., M.R., P.Q., A.R., R.E.K., M.A.C., S.A., V.M.P., M.Co, and S.V. Formal Analysis: D.C., T.B., P.Q., M.A.C., S.A., V.M.P., S.V., and I.M. Visualization: D.C., S.A., and S.V. Project administration: D.C., V.M.P., P.S., and A.L. Resources: D.C., V.M.P., and A.L. Supervision: I.M., T.C., M.Ca, and A.L. Funding acquisition: A.L. Writing—original draft: D.C. and A.L. Writing—review and editing: D.C., T.B., M.R., P.Q., A.R., R.E.K., M.A.C., S.A., V.M.P., M.Co., S.V., P.S., I.M., T.C., M.Ca., and A.L.

Competing interests

A.L. is a co-founder, equity holder, and consultant of nChroma Bio, a company developing epigenome editing applications. P.S. was an employee of nChroma Bio at the time the work was conducted and holds an equity interest in the company. A.L., D.C., T.B., A.R., and M.A.C. are inventors on patent applications related to the development of the polyfunctional editing strategy and improved ETR design, filed by IRCCS Ospedale San Raffaele and Fondazione Telethon ETS or by nChroma Bio. All other authors have no competing interests.

Additional information

Supplementary information The online version contains supplementary material available at https://doi.org/10.1038/s41467-026-72846-2.

Correspondence and requests for materials should be addressed to Angelo Lombardo.

Peer review information *Nature Communications* thanks Albert Jeltsch and the other, anonymous, reviewer(s) for their contribution to the peer review of this work. A peer review file is available.